Functional interplay between SA1 and TRF1 in telomeric DNA binding and DNA–DNA pairing

Jiangguo Lin[1,2], Preston Countryman[2], Haijiang Chen[3,4], Hai Pan[2], Yanlin Fan[3], Yunyun Jiang[3], Parminder Kaur[2], Wang Miao[5], Gisele Gurgel[6], Changjiang You[7], Jacob Piehler[7], Neil M. Kad[8], Robert Riehn[2], Patricia L. Opresko[9], Susan Smith[10], Yizhi Jane Tao[3] and Hong Wang[2,*]

[1]School of Bioscience and Engineering, South China University of Technology, Guangzhou, Guangdong 510006, P.R. China, [2]Physics Department, North Carolina State University, Raleigh, North Carolina, NC 27695, USA, [3]Department of BioSciences, Rice University, Houston, TX 77005, USA, [4]Institute of Microbiology and College of Life Sciences, Zhejiang University, Hangzhou, Zhejiang 310058, P.R. China, [5]Department of Neurology, The First Affiliated Hospital of Zhengzhou University, Zhengzhou, Henan 450014, P.R. China, [6]Biomanufacturing Training and Education Center, North Carolina State University, Raleigh, North Carolina, NC 27695, USA, [7]Division of Biophysics, Universität Osnabrück, Barbarstrasse 11, 49076 Osnabrück, Germany, [8]School of Biosciences, University of Kent, Canterbury, Kent CT2 7NJ, UK, [9]Department of Environmental and Occupational Health, University of Pittsburgh, PA 15213, USA and [10]Kimmel Center for Biology and Medicine at the Skirball Institute, Department of Pathology, New York University School of Medicine, New York, NY 10016, USA

ABSTRACT

Proper chromosome alignment and segregation during mitosis depend on cohesion between sister chromatids. Cohesion is thought to occur through the entrapment of DNA within the tripartite ring (Smc1, Smc3 and Rad21) with enforcement from a fourth subunit (SA1/SA2). Surprisingly, cohesin rings do not play a major role in sister telomere cohesion. Instead, this role is replaced by SA1 and telomere binding proteins (TRF1 and TIN2). Neither the DNA binding property of SA1 nor this unique telomere cohesion mechanism is understood. Here, using single-molecule fluorescence imaging, we discover that SA1 displays two-state binding on DNA: searching by one-dimensional (1D) free diffusion versus recognition through subdiffusive sliding at telomeric regions. The AT-hook motif in SA1 plays dual roles in modulating non-specific DNA binding and subdiffusive dynamics over telomeric regions. TRF1 tethers SA1 within telomeric regions that SA1 transiently interacts with. SA1 and TRF1 together form longer DNA–DNA pairing tracts than with TRF1 alone, as revealed by atomic force microscopy imaging. These results suggest that at telomeres cohesion relies on the molecular interplay between TRF1 and SA1 to promote DNA–DNA pairing, while along chromosomal arms the core cohesin assembly might also depend on SA1 1D diffusion on DNA and sequence-specific DNA binding.

INTRODUCTION

In eukaryotes, proper chromosome alignment and segregation during mitosis depend on cohesion between sister chromatids (1–4). Cohesion is mediated by the cohesin complex, which also plays important roles in other diverse biological processes, including double-strand DNA repair and maintenance of three-dimensional chromatin organization (5,6). In vertebrates, the core cohesin complex consists of a tripartite ring assembled by Smc1, Smc3, Rad21 (also known as Scc1) and the stromal antigen subunit (SA) SA1 (STAG1) or SA2 (STAG2) (3).

In addition to association at centromeres, cohesin complexes are distributed at low densities along chromosome arms (7). This observation implies a low coverage of cohesin rings at telomeres. Telomeres are nucleoprotein structures that prevent the degradation or fusion of linear chromosome ends by preventing them from activating the DNA damage response and double-strand DNA break repair machineries (8–11). Human telomeres contain ∼2–20 kb of TTAGGG repeats and a G-rich 3′ overhang (12). In humans, a specialized protein complex called shelterin (consisting of TRF1, TRF2, POT1, TIN2, TPP1 and RAP1) regulates telomerase access, DNA damage response and sister chromatid cohesion at telomeres (13–17). Aging or dis-

---

*To whom correspondence should be addressed. Tel: +1 919 513 7203; Fax: +1 919 515 6538; Email: hong_wang@ncsu.edu

ease associated telomere shortening contributes to genome instability and cancer progression by inducing chromosome end resection, fusion and breakage (18). G-quadruplex (G4) and intermediate structures present during G4 formation cause chromosome fragility and replication fork stalling at telomeres (19,20). However, the cohesion process can counteract these effects by facilitating the restart of stalled replication forks (6,21). This function highlights the important role that the cohesion process plays at telomeres.

Our previous studies revealed that SA1 is required for telomere cohesion whereas, SA2 is required at centromeres (22). Depletion analysis showed that telomeres relied heavily on SA1 and to a lesser extent on the ring for cohesion (23). While deletion of cohesin ring subunits or SA2 dramatically decreases cohesion at centromeres, it does not significantly affect sister telomere association (23). Furthermore, SA1, not SA2, functionally interacts with TRF1 and TIN2 (24). Beyond its function at telomeres, SA1 is enriched at promoters and CCCTC-binding factor (CTCF) sites, which in turn determines the distribution of cohesin complexes along chromosomes (25). However, the DNA binding properties of SA1, are unknown, but have important implications for advancing our understanding of the mechanism underlying sister chromatid cohesion and its contribution to chromosome architecture determination (26). Furthermore, it is unclear if SA1 specifically recognizes telomeric DNA sequences, or if TRF1 influences SA1's interactions with telomeric DNA. Importantly, it is not fully understood how sister telomere cohesion is achieved through SA1 in conjunction with the shelterin proteins TRF1 and TIN2.

Here, we used fluorescence imaging to study quantum dot- (QD-) labeled SA1 on DNA containing alternating telomeric and non-telomeric sequences. This platform was used to investigate how SA1 achieves DNA binding specificity for telomeric sequences by itself and in partnership with TRF1. We discovered that SA1 displays two-state binding on DNA: fast searching using one-dimensional (1D) unbiased diffusion and reading (recognition) at telomeric regions using a slow subdiffusive sliding mechanism. The N-terminal domain of SA1 (SA1-N) containing the AT-hook motif mediates both the non-specific binding and subdiffusive diffusion modes. Monte Carlo simulations using a two-state model for SA1 (free 1D diffusing during searching and pausing during reading) suggest that the slow subdiffusive behavior can be explained by higher probabilities of pausing events at telomeric sequences. Furthermore, we found that the presence of TRF1 tethers SA1 within the telomeric region, while individual SA1 molecules diffuse through multiple telomeric and non-telomeric regions on DNA tightropes. Using atomic force microscopy (AFM) imaging we found that TRF1 and SA1 together promote longer protein-mediated DNA–DNA pairing tracts compared with TRF1 alone. Taken together, these results directly revealed the molecular interplay between SA1 and TRF1 in telomeric DNA binding and in promoting DNA–DNA pairing during sister telomere cohesion. Importantly, these results strongly suggest a new model for cohesin assembly that takes into consideration the 1D diffusion of SA1 on DNA and its sequence specific binding.

MATERIALS AND METHODS

Protein-QD conjugation

Streptavidin-conjugated quantum dots (SAv-QDs) and secondary antibody-coated quantum dots (Ab-QDs) were purchased from Invitrogen. Flag and SUMO antibodies were purchased from Sigma and Santa Cruz Biotechnology, respectively. For labeling N-terminal 3X Flag-tagged WT SA1, SA1 R37A R39A (GenScript), or SUMO-tagged SA1-N (SA1-N, 1–72 AA), QDs (1 μl of 1 μM) were incubated with the primary antibodies (1 μl of 1 μM) for 20 min. Proteins (1 μl, 0.7 μM Flag-SA1 or 1 μM SUMO-SA1-N) were added to the solution and incubated for an additional 20 min. For single-color QD labeling of N-terminal His$_6$-tagged full length SA1 (His-SA1), 1 μl of SAv-QD (1 μM, Invitrogen) was incubated with 1 μl of the multivalent chelator tris-nitrilotriacetic acid (^{BT}tris-NTA, 2 μM) for 20 min (27). His-SA1 protein (1 μl of 1 μM) was then added to the SAv-QD-NTA solution and incubated for an additional 20 min. Experiments were carried out using equal molar concentration of green (565 nm) and red (655 nm) QDs. A higher percentage of dual-color labeling of Flag-SA1 molecules (46%, $N = 107$) was present compared to His-SA1 (10%, $N = 67$). This difference is most likely due to the simultaneous binding of two Ab-QDs to the 3X Flag tag on SA1. For dual-color differential labeling of Flag-SA1 and N-terminal His-tagged TRF1 (His-TRF1), additional His-tagged single-chain antibody fragments (2 μl of 5 μM) and dithiothreitol (DTT, 5 μl of 2 mM) were added sequentially to the SA1-QD solution and incubated for 20 min at each step. The addition of DTT and the antibody fragments is to prevent His-TRF1 from non-specifically binding to Ab-QDs through the metal-histidine coordination (28). The Flag-SA1-QDs and His-TRF1-QDs were prepared separately, then mixed and incubated for an additional 20 min. All samples were diluted 200$\times$ for WT SA1 and 20$\times$ for SA1 R37A R39A mutant protein, before being introduced into the flow cell in the imaging buffer [20 mM Tris (pH 7.5), 100 mM KCl and 0.1 mM MgCl$_2$]. Formation of dual-color QD-labeled complexes on T270 tightropes depends on the presence of both TRF1 and SA1, which shows that the crosstalk between His-TRF1 and Ab-QDs is not significant.

AFM imaging and analysis

All DNA and protein samples were diluted in 1$\times$ AFM buffer [25 mM HEPES–KOH (pH 7.5), 25 mM NaOAc and 10 mM Mg(OAc)$_2$] before being deposited onto freshly cleaved mica surface (SPI Supply). Then, the samples were washed with MilliQ water and dried under a stream of nitrogen gas. The final protein, QD and DNA concentrations were 6.7 nM, 6.7 nM and 0.58 μg/ml, respectively. When QDs were not included, the final concentrations of SA1 and TRF1 proteins were 30 and 50 nM, respectively. All images were collected in the AC mode using a MFP-3D-Bio AFM (Asylum Research). Pointprobe$^®$ PPP-FMR probes (Nanosensors) with spring constants at ~2.8 N/m (nominal value) were used. All images were captured at a scan size of 1–3 $\times$ 1–3 μm, a scan rate of 1–2 Hz and a resolution of 512 $\times$ 512 pixels. The positions of proteins and protein-QDs on

DNA were analyzed using the software from Asylum Research.

Fluorescence imaging and analysis

The oblique angle total internal reflection microscopy based particle tracking of QD-labeled proteins on DNA tightropes was described previously (29).

The mean square displacement (MSD) as a function of time interval is given by:

$$\text{MSD}(n\Delta t) = \frac{1}{N-n}\sum_{i=1}^{N-n}\left[(x_{i+n}-x_i)^2 + (y_{i+n}-y_i)^2\right] \quad (1)$$

where N is the total number of frames in the trajectory, n is the number of frames for different time intervals, Δt is the time between frames and x_i and y_i are the positions of the protein-QD in the frame i. The 1D diffusion constant (D) and diffusion exponent (alpha factor) were analyzed by a custom routine developed in LabView Software based on the following equation (30):

$$\text{MSD} = 2Dt^{\alpha} \quad (2)$$

A protein was categorized as being mobile if the diffusion constant was greater than 5×10^{-4} $\mu m^2/s$ and R^2 value from data fitting using Equation (2) was >0.8. To detect slow diffusion events on DNA based on the time interval-based diffusion constant (D_{int}), we developed a custom MATLAB code to execute 'sliding window' (40-frame, 2 s) MSD analysis (31).

RESULTS

Full length SA1 binds specifically to telomeric DNA sequences

Recently, we demonstrated that the N-terminal domain of SA1 (1-72 AA, SA1-N) binds to a DNA substrate containing telomeric sequences (23). However, whether or not the full length SA1 binds specifically to telomeric DNA was unknown. To understand the SA1 DNA binding mechanism, we obtained full length His- and Flag-tagged SA1 proteins using the baculovirus/insect cell expression system (Supplementary Methods and Supplementary Figure S1A). On a gel filtration column, the full length His-SA1 eluted at a mean volume consistent with a monomeric protein (Supplementary Figure S1B). Fluorescence anisotropy experiments demonstrated that the equilibrium dissociation constant of SA1 for a duplex DNA substrate containing 7 TTAGGG repeats ($K_d = 34.0 \pm 5.8$ nM, mean $\pm$ SEM) was ~3-fold lower than that obtained for a DNA substrate of the same length but with scrambled sequences ($K_d = 104.0 \pm 13.6$ nM, Figure 1A). In contrast, SA1 did not show specificity for CTCF consensus sequences (Supplementary Figure S2). To study SA1 binding to longer telomeric substrates, we carried out AFM imaging and statistical analysis ('Materials and Methods' section) of the binding position of SA1 on a telomeric DNA substrate containing 270 TTAGGG repeats (T270, 5.4 kb) and a control substrate (3.8 kb) containing only the non-telomeric (genomic) DNA sequences from T270 (Figure 1B). AFM imaging indicated that a higher percentage (41.9%) of SA1 bound at the telomeric region on

the T270 DNA substrate compared to the same locations along the genomic DNA substrate (27.0%). In summary, both fluorescence anisotropy and AFM imaging showed that full length SA1 binds to telomeric sequences with weak (~2- to 3-fold) specificity.

SA1 alternates between fast and slow diffusion on DNA containing telomeric sequences

Dynamic movements on DNA, such as 1D sliding (translocation while maintaining continuous DNA contact), jumping and hopping (microscopic dissociation and rebinding events) are essential for a protein to find its target sites on DNA (32–37). To further understand how SA1 dynamically achieves DNA binding specificity for telomeric sequences, we used oblique angle fluorescence microscopy imaging of QD-labeled proteins on T270 DNA tightropes containing alternating telomeric and genomic regions ('Materials and Methods' section) (29,38–41). Hydrodynamic flow was used to stretch DNA and suspend ligated T270 DNA strands between poly-L-lysine coated silica microspheres at an elongation of ~90% of the DNA contour length (Figure 2A and Supplementary Methods) (29). We conjugated Flag-SA1 to secondary antibody-coated QDs (Ab-QDs) using an antibody sandwich method (Figure 1C) (27).

AFM imaging revealed that Ab-QDs without SA1 did not have significant binding affinity for T270 DNA, and SA1-QDs retained binding specificity for telomeric sequences (Figure 1C). The binding of SA1-QDs molecules to DNA was long lived, with 78.5% ($N = 107$) of SA1-QD complexes remaining on T270 DNA tightropes after 2 min (Supplementary Figure S3A). Analysis of SA1 on T270 DNA revealed two populations (Figure 2B–D): static and mobile molecules. Surprisingly, while some mobile SA1 molecules displayed free 1D diffusion on T270 DNA throughout the entire observation period (2 min, Figure 2C), a subpopulation of mobile SA1 molecules alternated between periods of slow and fast diffusion (Figure 2D and Supplementary Movie S1). His-SA1-QDs also displayed bimodal diffusion behavior (fast and slow diffusion) on T270 DNA (Supplementary Figure S3B). These results indicate that this type of bimodal diffusion behavior (fast and slow diffusion) is independent of QD conjugation strategies.

The diffusion range of SA1 molecules on T270 DNA tightropes covered distances from ~0.18 to 8.55 μm (~6 ligated T270 molecules), with some SA1 molecules visiting more than one telomeric segment (1.6 kb each, Figure 2D). Strikingly, some SA1 molecules repeatedly slowed down at the same regions along T270 DNA tightropes, manifested as distinct peaks in the position histogram of SA1 along DNA (Figure 2D, top panel). The distribution of the pairwise distances between these peaks exhibited two populations centered at 0.5 and 1.5 μm (Figure 2E). These distances are consistent with the boundaries of the telomeric region (1.6 kb) and the spacing between two adjacent telomeric regions on T270 DNA (5.4 kb), respectively. Furthermore, we also observed the alternation between fast and slow diffusion of SA1 at lower (50 mM KCl) and higher (150 mM KCl) salt concentrations (Supplementary Figure S4). Collectively, these results show that SA1 alternates be-
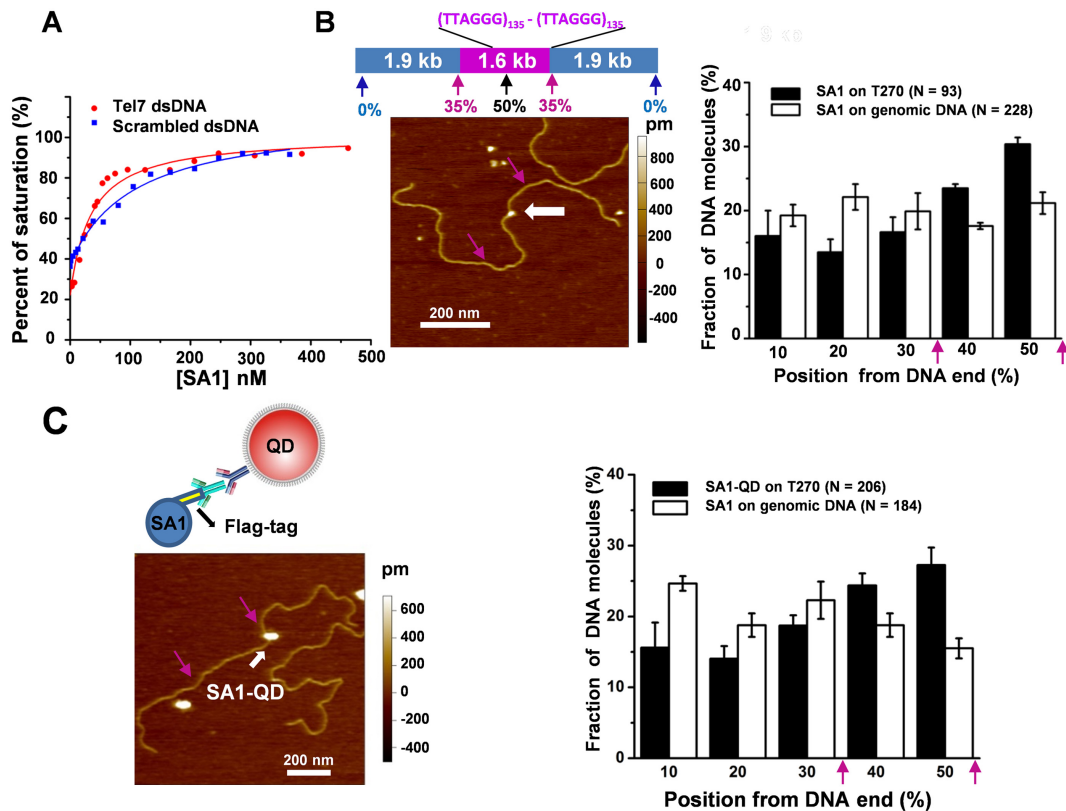
Figure 1. Full length SA1 and SA1-QDs bind to telomeric DNA sequences with weak specificity. (**A**) Fluorescence anisotropy experiments showing concentration-dependent binding of 3xFlag-tagged SA1 (Flag-SA1) to DNA substrates containing 7 TTAGGG repeats (Tel7, red dots) or scrambled DNA sequences (blue dots). The data were fitted to the law of mass action (Supplementary Methods). The equilibrium dissociation constants are 34.0 (±5.8) and 104.0 (±13.6) nM, respectively, for DNA substrates with telomeric and scrambled sequences (two independent experiments). (**B** and **C**) Representative AFM images (left panels) and statistical analysis of the full length Flag-SA1 (**B**) and SA1-QDs (**C**) (white arrows) binding to the T270 DNA substrate, excluding the end binding events. Schematic drawings of the T270 DNA substrate and the QD conjugation strategy (an antibody-sandwich method for the full length Flag-SA1) are shown in the top panels in B and C, respectively. The purple arrows point to the estimated boundaries between the genomic and telomeric sequences. Each dataset was from at least three independent experiments with error bars representing SEM.

tween fast and slow diffusion on DNA tightropes containing telomeric and non-telomeric sequences. The pairwise distance between slow diffusion events on T270 DNA indicates that slow diffusion events are more likely to occur at telomeric regions.

Long SA1 slow diffusion events depend on telomeric sequences

To investigate whether the slow diffusion events displayed by SA1 on DNA depend on the presence of TTAGGG repeats, we imaged QD-labeled SA1 on DNA tightropes containing only the genomic sequence portion of the T270 DNA substrate or centromeric DNA sequences (Figure 3A). On genomic and centromeric DNA tightropes, SA1 molecules showed different DNA binding dynamics compared with T270 DNA (Figure 3). The percentage of SA1 molecules displaying static binding on T270 DNA was ∼3- and 9-fold higher than on genomic and centromeric DNA, respectively (Figure 3B).

To further compare the dwell times of the slow diffusion events displayed by mobile SA1 on different DNA substrates, we used 'sliding window' (40-frame, 2 s) MSD analysis to calculate a time interval-based diffusion con-

stant (D_{int}, bottom panels in Figure 2C and D) (31). Distinct from static ($<0.5 \times 10^{-3}$ μm^2/s, Supplementary Figure S5A) and fast free diffusion modes ($>10 \times 10^{-2}$ μm^2/s, Supplementary Figure S5B), this analysis indicated that mobile SA1 molecules with fast and slow diffusion on T270 DNA show a distinct peak at ∼1.0×10^{-3} μm^2/s (Supplementary Figure S5C). Therefore, for calculating dwell times on DNA tightropes we used D_{int} value of 5.0×10^{-3} μm^2/s as the threshold to identify individual slow diffusion events. This D_{int} based analysis showed that the dwell times of individual SA1 slow diffusion events on T270 (1.17 s) are significantly ($P < 0.05$) longer than on genomic (0.80 s) and centromeric (0.79 s) DNA (Supplementary Figure S6A). The percentage of mobile SA1 molecules showing long slow diffusion events ($D_{in} < 5.0 \times 10^{-3}$ μm^2/s for longer than 2 s) on T270 DNA (51.2%) was at least ∼2-fold higher than on genomic (17.6%) or centromeric DNA (24.1%, Figure 3C, Table 1). Furthermore, among all mobile SA1 molecules analyzed, SA1 spent a significantly larger percentage of time (24.4%) in the slow diffusion mode on T270 DNA than on genomic (3.2%) and centromeric DNA (6.3%, Supplementary Figure S6B).

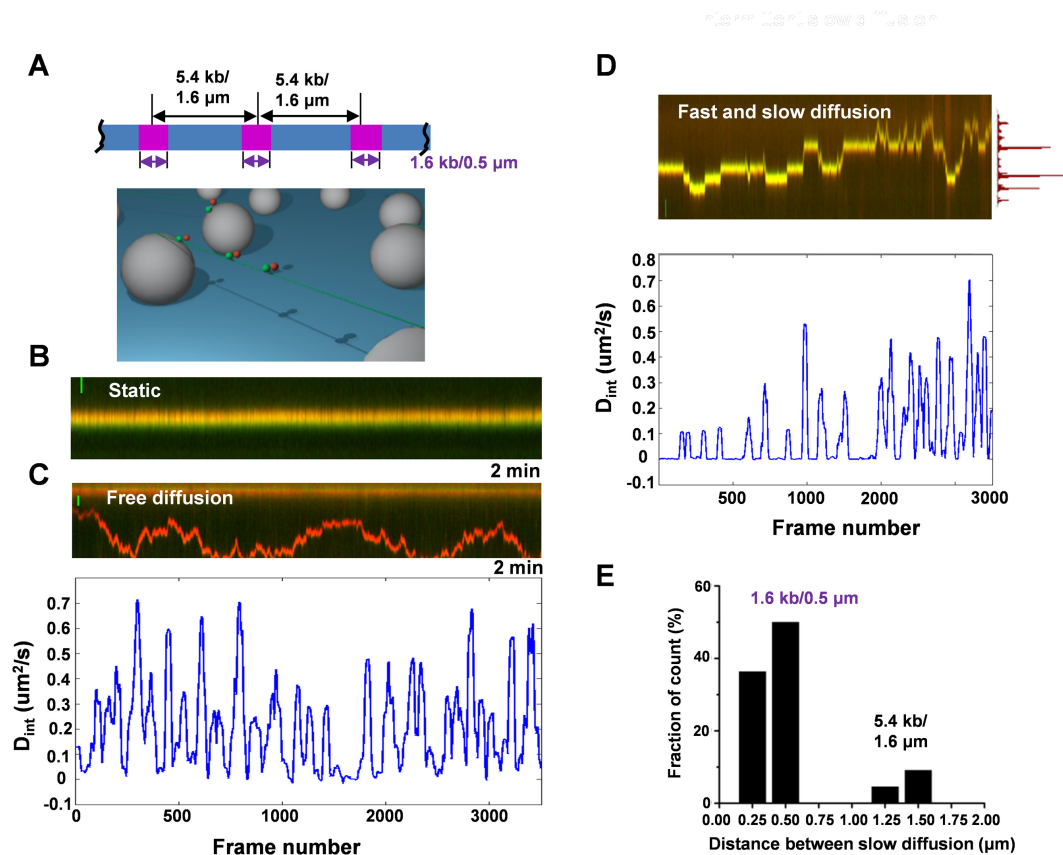Using MSD analysis we further compared the dynamics of SA1 on different DNA substrates. SA1 displayed sig-

Figure 2. Full length SA1 alternates between fast and slow 1D diffusion on T270 DNA tightropes. (**A**) Ligated T270 DNA substrate (top panel) and the DNA tightrope assay setup (bottom panel). (**B–D**) Dynamics of the full length Flag-SA1 on T270 DNA tightropes. Kymographs of SA1 molecules being static (B), showing free 1D diffusion (C), and alternating between fast and slow 1D diffusion (D) on T270 DNA. Scale bars (y-axis): 1 μm. Equimolar concentrations of red (655 nm) and green (565 nm) QDs were used in SA1 conjugation. The bottom panels in C and D show corresponding plots of diffusion constants (D_{int}) based on the 40-frame sliding window (2 s) MSD analysis. Each frame is 50 ms. The histogram on the right side of the top panel in D shows the position distribution of SA1 along the T270 DNA tightrope. (**E**) The distribution of pair-wise distance between nearest SA1 slow diffusion positions ($N = 22$).

nificantly ($P < 0.005$) slower diffusion constants on T270 DNA (0.04 ± 0.01 μm²/s) in comparison with DNA substrates containing genomic (0.14 ± 0.03 μm²/s) or centromeric (0.11 ± 0.02 μm²/s) DNA sequences (Table 1). In addition, we calculated the diffusive exponent (alpha factor) to determine whether SA1 displays subdiffusive motion on DNA (Table 1). An alpha factor of 1 indicates an unbiased random walk and a value less than 1 indicates periods of pausing in the random walk (subdiffusion) (30). On T270 DNA, SA1 displayed significantly ($P < 0.001$) smaller alpha factors (0.69 ± 0.03) compared to genomic (0.89 ± 0.02) and centromeric (0.82 ± 0.02) DNA substrates (Table 1). In summary, fluorescence imaging of QD-labeled proteins established that SA1 alternates between slow and fast diffusion on DNA. These slow diffusion events are telomere sequence dependent. Additionally, the alpha factor for SA1 on T270 was significantly smaller than on genomic DNA, which suggests protein pausing amid free diffusion at telomeric sequences.

SA1 slow diffusion events are mediated through its N-terminal domain

SA1 contains a unique AT-hook motif at its N-terminal domain, which is not present on SA2 (23). The AT-hook domain has been proposed to serve as an accessory domain for transcription factors to bind specific-DNA sequences/structures (42). To determine whether or not SA1 slow diffusion events depend on its unique N-terminal domain, we purified the SUMO-tagged SA1 N-terminal fragment (SA1-N) (23). Analysis of the binding position of SA1-N on T270 DNA in AFM images demonstrated that SA1-N binds specifically to the telomeric regions (Figure 4A and Supplementary Figure S7A). These results are consistent with previous electrophoresis mobility shift assays (EMSAs) indicating SA1-N binding to telomeric sequences (23).

For fluorescence imaging, we labeled N-terminal SUMO-tagged SA1-N with Ab-QDs through a primary antibody against the SUMO tag (Figure 4B and Supplementary Methods). Consistent with results from AFM imaging, incubation of SA1-N-QDs with T270 DNA tightropes resulted in substantial DNA binding. Importantly, SA1-N also displayed slow diffusion events on T270 DNA (Fig-
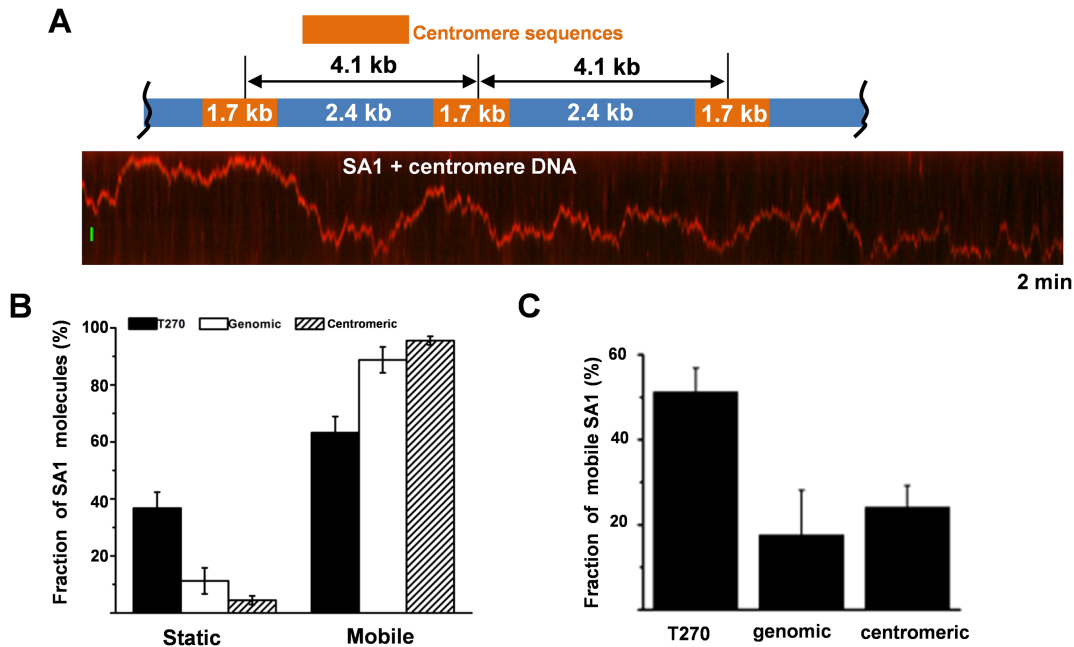
Figure 3. Long slow diffusion events by SA1 on DNA depend on the presence of telomeric sequences. (**A**) Dynamics of the full length Flag-SA1 on DNA tightropes containing centromeric sequences. Top: a schematic drawing of the ligated DNA substrate containing centromeric sequences. Bottom: a kymograph showing a mobile QD-labeled Flag–SA1 complex on the centromeric DNA tightrope. The scale bar (y-axis): 1 μm. (**B**) Comparison of the static and mobile SA1 populations on telomeric, genomic and centromeric DNA tightropes. The percentages of static SA1 molecules are 36% ($N = 84$), 11% ($N = 63$) and 4% ($N = 97$) on telomeric, genomic and centromeric DNA, respectively. (**C**) The percentages of SA1 (out of all mobile molecules) with long slow diffusion events (>2 s) on telomeric, genomic and centromeric DNA. The mean values are 51.2% ($N = 54$), 17.6% ($N = 56$) and 24.1% ($N = 93$), for telomeric, genomic and centromeric DNA substrates, respectively (from two or three independent experiments). The error bars represent SEM.

ure 4C and Supplementary Movie S2). The static binding and long slow diffusion events (>2 s) on T270 displayed by SA1-N also were telomeric sequence dependent (Supplementary Figure S7B and C). A significantly higher percentage of SA1-N molecules (74.3%) showed slow diffusion events (dwell time > 2 s) on T270 DNA than on genomic DNA (38.6%). Consistent with these results, the diffusion constant of mobile SA1-N on T270 DNA (0.06 ± 0.01 μm^2/s) was significantly ($P = 0.001$) lower than that on genomic DNA (0.12 ± 0.02 μm^2/s, Table 1). Furthermore, the alpha factor of SA1-N 1D diffusion (0.74 ± 0.03) was significantly smaller ($P < 0.001$) on T270 than on genomic DNA (0.89 ± 0.02, Table 1).

Previously, it was shown that the mutations at the central core sequence (KRK**R**G**R**P) in the SA1 AT-hook motif (SA1-N R37A R39A) significantly reduces its binding to telomeric DNA (23). To further understand the role of SA1's AT-hook motif in DNA binding, we obtained the full length Flag-tagged SA1 R37A R39A mutant (Supplementary Figure S1A). Fluorescence anisotropy experiments showed that the double mutations at the AT-hook domain reduced the K_d of SA1 for genomic DNA and telomeric DNA by ∼9.3- and 6.5-fold, respectively (Figure 4D). Intriguingly, on the control DNA tightropes containing non-specific genomic and centromeric sequences, QD-labeled SA1 R37A R39A diffused significantly slower (0.03 ± 0.01 μm^2/s, $P < 0.0003$) than the WT protein (0.11 ± 0.02 μm^2/s, Table 1). These results demonstrated that the core AT-hook motif plays an important role in nonspecific DNA binding and in promoting mobility of SA1

on DNA. Meanwhile, it is worth noting that SA1 R37A R39A still showed specificity (∼4×) for telomeric sequences (7 TTAGGG repeats), even though the overall DNA binding was reduced (Figure 4D). At the single-molecule level, QD-labeled SA1 R37A R39A also displayed alternating slow and fast diffusion events on T270 DNA tightropes (Figure 4C). However, compared to the WT protein, the ability of SA1 R37A R39A to carry out subdiffusive diffusion on DNA is significantly compromised. Compared to the WT protein (Table 1), the percentage of mobile SA1 R37A R39A molecules showing slow diffusion events (>2 s, 34%, $N = 86$) was significantly decreased for both telomeric and centromeric DNA substrates. In addition, the alpha factor of SA1 R37A R39A on T270 (0.79 ± 0.05) was significantly higher ($P < 0.003$, Table 1) than that for WT SA1. In addition, with R37A R39A mutations, the difference between alpha factors displayed by SA1 on T270 (0.79 ± 0.05) and the control DNA substrate (0.83 ± 0.03) was diminished (Table 1). Collectively, the fluorescence anisotropy and single-molecule fluorescence imaging results demonstrated the dual roles of the central core sequence (KRK**R**G**R**P) at the AT-hook motif in achieving high affinity nonspecific SA1 DNA binding and modulating telomere sequence dependent subdiffusive behavior on DNA.

SA1 becomes subdiffusive or static within telomeric regions in the presence of TRF1

SA1 interacts directly with TRF1 through its N-terminal domain (24). EMSAs using a DNA substrate containing 3
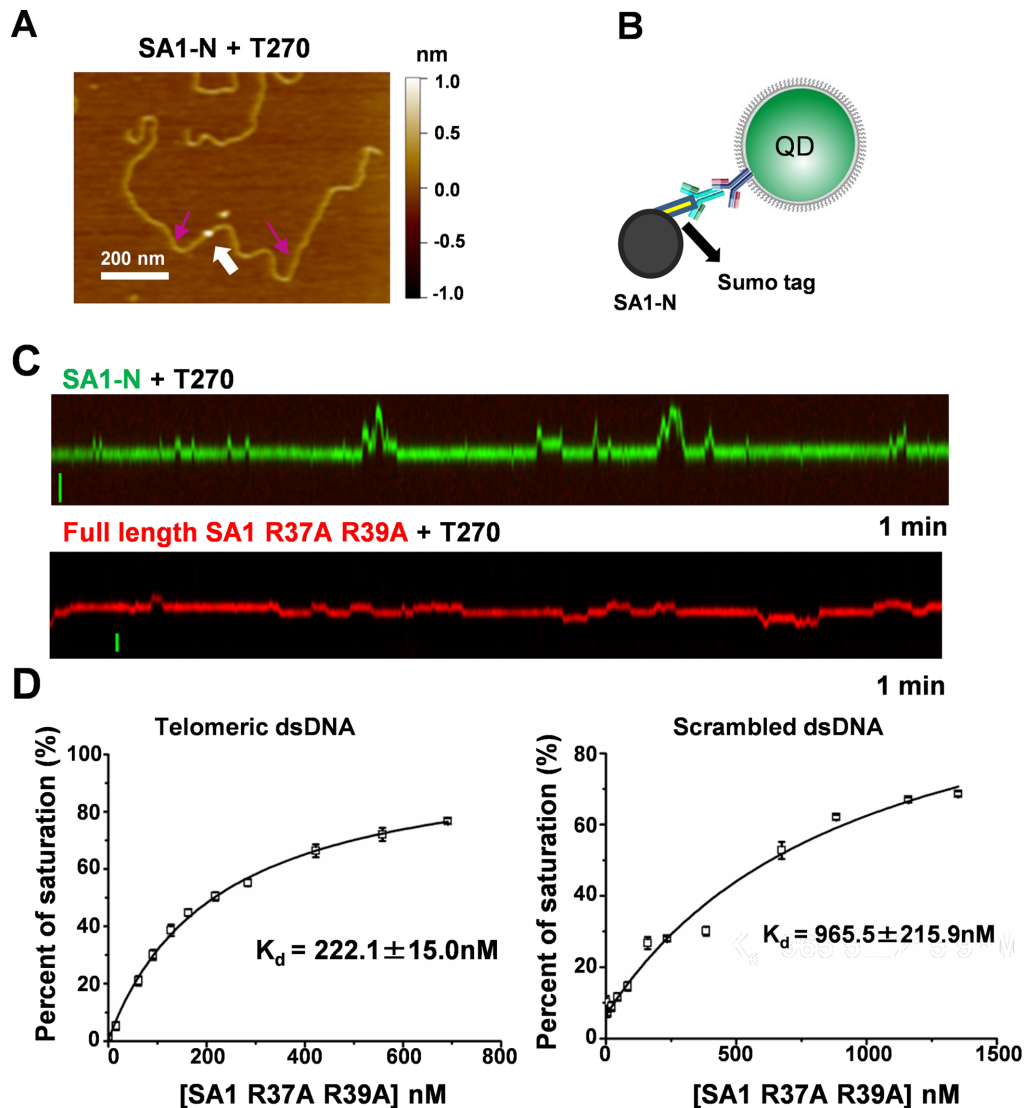
Figure 4. The AT-hook motif in SA1 mediates non-specific DNA binding and subdiffusive dynamics on telomeric T270 DNA substrate. (**A**) A representative AFM image showing SA1-N (white arrow) binding to T270 DNA. The purple arrows point to the estimated boundaries of the telomeric region. (**B**) QD conjugation strategy: an antibody-sandwich method for Sumo-tagged SA1-N. (**C**) Kymographs of QD-labeled SA1-N (green, top panel) and full length SA1 R37A R39A (red, bottom panel) on T270 DNA tightropes. Scale bars (y-axis): 1 μm. (**D**) Fluorescence anisotropy experiments showing concentration-dependent binding of 3xFlag-tagged SA1 R37A R39A to DNA substrates containing 7 TTAGGG repeats (Tel7, left panel) or scrambled DNA sequences (right panel). The data were from two independent experiments.

TTAGGG repeats showed that TRF1 and SA1 together induced a supershift relative to TRF1-DNA and SA1–DNA complexes (Figure 5A). This result suggests that TRF1 and SA1 can interact simultaneously with the same piece of DNA.

To evaluate how TRF1 affects the dynamics of SA1 on DNA, we directly imaged their interactions. Flag-SA1 and His-TRF1 proteins were orthogonally conjugated with red Ab-QDs and green SAv-QDs via antibody sandwich and [BT]tris-NTA linkage strategies, respectively (Figure 5B and Supplementary Movie S3). Under these conditions, 11.2% of the total protein-QDs on T270 DNA tightropes were dual-color labeled, which were dependent on the presence of both TRF1 and SA1 (Supplementary Figure S8A). A higher population of dual-colored SA1–TRF1–QD com-

plexes ($\sim$60%) were static than the single-colored SA1-QD alone ($\sim$35%) on T270 DNA tightropes (Figure 5D). On T270 DNA tightropes, the majority (68.2%) of the mobile SA1–TRF1 complexes diffused within a range less than the length of telomeric region ($\sim$0.5 μm) during the entire observation time window (2 min, bottom panel of Figure 5C and E). In stark contrast, the majority (73.3%) of SA1 alone molecules (single-color labeled) diffused through multiple telomeric and non-telomeric regions (with diffusion ranges > 0.5 μm, Figure 5C (top panel) and E). These results suggest that the narrow diffusion range displayed by SA1–TRF1 is due to interactions between TRF1 and SA1. To further confirm that the confined motion displayed by SA1–TRF1 is telomeric sequence dependent, we studied the diffusion range of dual-colored SA1–TRF1–QDs
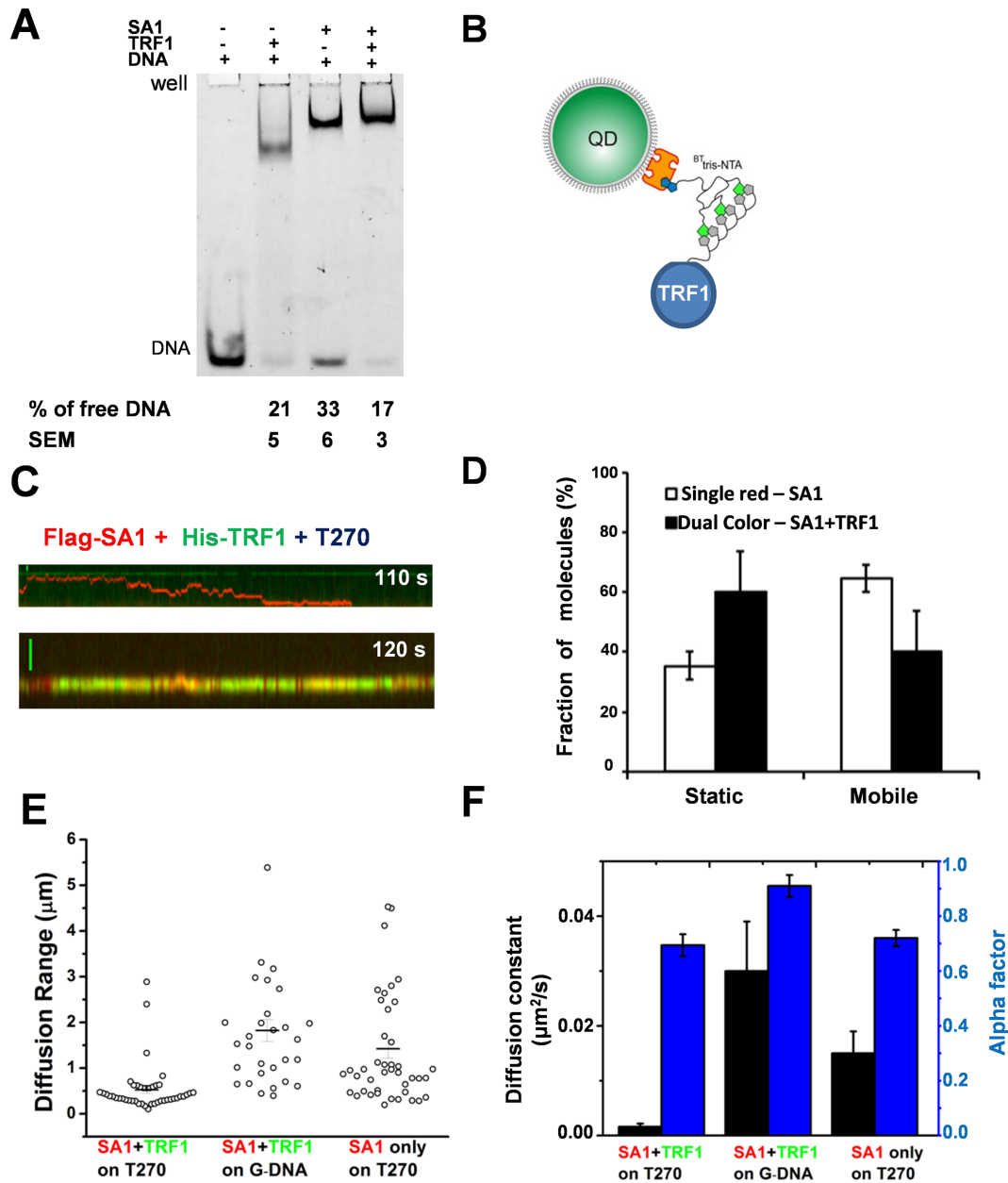
Figure 5. TRF1 tethers SA1 within a telomeric region on DNA. (**A**) EMSA of TRF1 (350 nM) and SA1 (350 nM) in the presence of the Alexa 488-labeled DNA substrate containing three TTAGGG repeats (5 nM). (**B**) Schematic drawing of QD-labeling for TRF1 using the ^{BT}tris-NTA linkage strategy. (**C**) Kymographs of Flag-SA1 and His-TRF1 proteins differentially conjugated with red Ab-QDs and green SAv-QDs using the antibody sandwich (Figure 1C) and ^{BT}tris-NTA linkage strategies, respectively. SA1-QDs (43.8 nM) and TRF1-QDs (62.5 nM) were incubated together for 20 min before being diluted and injected into the flow cell containing DNA tightropes. (**D**) On T270 tightropes, dual-color labeled SA1–TRF1 complexes display a higher percentage of static complexes, compared to SA1 alone (red QD-labeled). The percentage of static complexes is 35% ($\pm$4%, N = 44) for SA1 only and 60% ($\pm$14%, N = 47) for SA1–TRF1 complexes. (**E**) Dual-color QD-labeled SA1–TRF1 complexes are confined within a short range on T270 DNA, but not on genomic DNA (G-DNA). Dual-color labeled SA1–TRF1 complexes on T270 display a higher percentage of complexes (68.2%, N = 44) with diffusion range less than 0.5 μm, compared to SA1 alone on T270 (red QD-labeled, 26.7%, N = 43) or dual colored SA1–TRF1 on the genomic DNA (6.7%, N = 30). (**F**) On T270, dual color-labeled SA1–TRF1 complexes show slower diffusion constants ($D = 0.0016 \pm 0.0006$ μm^2/s, N = 44) and smaller alpha factors (0.69 $\pm$ 0.04), compared to complexes on genomic DNA (G-DNA, $D = 0.03 \pm 0.009$ μm^2/s, alpha factor = 0.91 $\pm$ 0.04, N = 30). Each dataset was from at least three independent experiments.

Table 1. Summary from analysis of diffusion dynamics of QD-labeled full length WT SA1, SA1-N and SA1 R37A R39A on DNA tightropes

DNA	WT SA1-QDs				SA1-N-QDs				SA1 R37A R39A		
	D (μm²/s)	Alpha factor	%	N	D (μm²/s)	Alpha factor	%	N	D (μm²/s)	Alpha factor	N
T270	0.04 ± 0.01 (0.02 to 0.06)	0.69 ± 0.03 (0.63–0.75)	51.2% (N = 54)	48	0.06 ± 0.01 (0.04–0.08)	0.74 ± 0.03 (0.68–0.80)	74.3% (N = 88)	103	0.03 ± 0.01 (0.01–0.05)	0.79 ± 0.05 (0.69–0.89)	33
Genomic	0.14 ± 0.03 (0.08 to 0.20)	0.89 ± 0.02 (0.85–0.93)	17.61% (N = 55)	36	0.12 ± 0.02 (0.08–0.16)	0.89 ± 0.02 (0.85–0.93)	38.6% (N = 103)	160			
Centromeric	0.11 ± 0.02 (0.07–0.15)	0.82 ± 0.02 (0.78–0.86)	24.1% (N = 93)	75					0.03 ± 0.01 (0.01 to 0.05)	0.83 ± 0.03 (0.77–0.89)	36

Note: D: diffusion constant (mean ± SEM).
%: percentage of mobile molecules with long slow diffusion events (>2 s).
N: numbers of molecules analyzed for diffusion constant and alpha factors calculations.
The numbers in the parenthesis represent confidence intervals at the 95% confidence level.

on genomic DNA. Strikingly, on genomic DNA, only 6.7% of mobile SA1–TRF1 protein complexes were confined to a range <0.5 μm (Figure 5E). Furthermore, the distance between dual-color QD-labeled SA1–TRF1 complexes and green QD-labeled TRF1 was consistent with that of SA1–TRF1 complexes binding to telomeric regions (Supplementary Figure S8B). Therefore the restricted diffusion range is not a property of SA1–TRF1–QDs, but instead is related to the DNA binding energy landscape over telomeric DNA sequences. In addition, the diffusion constant and alpha factor of mobile SA1–TRF1 complexes were significantly ($P < 0.05$) smaller on T270 DNA than on genomic DNA tightropes (Figure 5F). Taken together, these results reveal that TRF1 is required to hold SA1 at the telomeric region.

SA1 and TRF1 together facilitate DNA–DNA pairing

TRF1 forms protein filaments on DNA and promotes parallel pairing of telomeric tracts (43). To elucidate the role of SA1–TRF1 interactions in sister telomere cohesion, we used AFM to investigate whether or not SA1 influences TRF1 mediated DNA–DNA pairing. Consistent with previous results (43), we observed that TRF1 molecules formed protein tracts that mediate DNA–DNA pairing on T270 DNA (Figure 6A). TRF1 protein tracts displayed average heights of 0.73 (± 0.10, mean ± SD) nm and average tract lengths of 66 (±4) nm (Figure 6D and Supplementary Figure S9). In contrast to TRF1 (50 nM), no protein tracts were observed when SA1 alone (30 nM) was incubated with T270 DNA. Importantly, in the presence of both TRF1 and SA1 (Figure 6B and C), the average SA1–TRF1-mediated DNA–DNA pairing tract length increased significantly to 92 (±7) nm (Figure 6D and Supplementary Figure S9). Due to its larger molecular weight, SA1 (142 kDa) on T270 DNA can be identified as individual proteins with heights (1.39 ± 0.50 nm, mean ± SD) significantly ($P < 0.05$) higher than TRF1 protein tracts (Supplementary Figure S9C). The location of SA1 on TRF1-mediated DNA–DNA pairing tracts was random. In the presence of SA1 R37A R39A and TRF1, the protein-mediated tract on T270 substrate ($78 ± 7$ nm, $N = 16$) was comparable with TRF1 alone. This result is consistent with our previous observation based on telomere fluorescence *in situ* hybridization showing that SA1 R37A R39A mutations abrogate the ability of SA1 to induce persistent cohesion at telomeres (23). In summary, SA1 and TRF1 together promote DNA–DNA pairing and the enhancement of TRF1-mediated DNA–DNA pairing depends on DNA binding by SA1.

Coarse-grained molecular dynamics (MD) simulations of synergistic effects of TRF1 and SA1 DNA binding

To further test the model that SA1 and TRF1 together bind to telomeric DNA and promote DNA–DNA pairing, we performed coarse-grained molecular dynamics (MD) simulations using HOOMD-blue (Supplementary Methods) (44). SA1 is modeled as a cubic, rigid domain that carries a DNA-binding site within a groove (Figure 7A). The groove enables SA1 to diffuse along DNA, but prevents bound molecules from bypassing each other. A previous electron microscopy study showed that a TRF1 dimer can simulta-
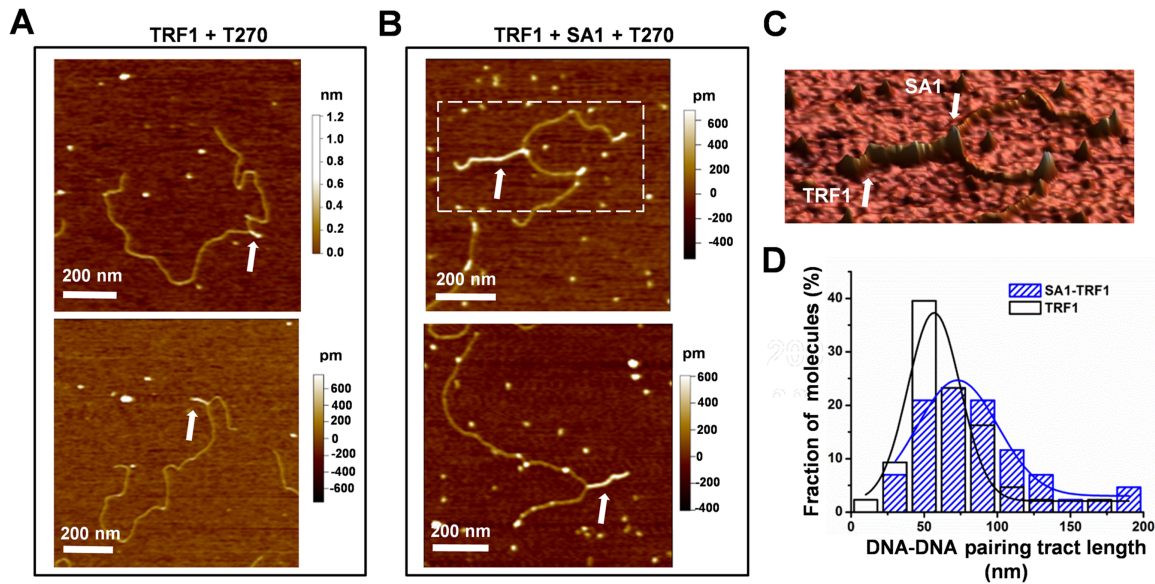
Figure 6. SA1 facilitates TRF1-mediated DNA–DNA pairing. (**A** and **B**) AFM images of T270 DNA (6.7 nM) in the presence of TRF1 only (50 nM) (A), or both TRF1 (50 nM) and SA1 (30 nM) (B). The white arrows point to the protein complex mediated DNA–DNA pairing. (**C**) A 3D image of the zoomed region from the top panel in B. (**D**) Protein tract lengths in the presence of only TRF1 (white bars) or both SA1 and TRF1 (blue bars). SA1 and TRF1 together increase the DNA–DNA pairing tract lengths to 92 ± 7 nm ($N = 50$) from 66 ± 4 nm ($N = 40$) for TRF1 alone. Each T270 DNA length was normalized to the mean length of the T270 DNA substrate (1.70 μm).

neously bind two DNA binding sites with only loose constraints on the distance or orientation between these two sites (45). Therefore, we constructed a TRF1 model containing a DNA binding domain similar to SA1 (representing the Myb domain), a flexible linker and a dimerization domain which also carries an anionic group (charge bead representing the acidic N-terminal domain, Figure 7B). We modeled the interaction between SA1 and TRF1 by allowing heterodimerization between the two proteins at the DNA-binding domain. Two 1800 bp DNA strands were modeled as semi-flexible strings of anionic 1-nm beads, which carry blocks corresponding to high affinity binding regions representing telomeric DNA sequences (1200 bp) and low affinity binding regions representing genomic DNA (600 bp). Based on previous studies of TRF1 DNA binding and fluorescence anisotropy measurements of SA1 DNA binding affinity (Figure 1A) (46,47), DNA binding constants where chosen so that binding energies followed the order: (TRF1 on genomic) < (SA1 on genomic) < (SA1 on telomeric) < (TRF1 on telomeric DNA).

Initially, we used MD simulations to establish TRF1 DNA binding modes that included TRF1 dimer-mediated DNA–DNA pairing (Figure 7C, left panels) (43). Next, we simulated SA1–DNA binding (Supplementary Figure S10A) and tested two computational scenarios: SA1 + TRF1 with heterodimerization (Figure 7C, right panels and Supplementary Figure S10B) and SA1 + TRF1 without heterodimerization. Under the simulation conditions, when only SA1 was present in the simulations, 34% of SA1 was bound to DNA (Supplementary Figure S10A). In stark contrast, in the scenario of heterodimerization between SA1 and TRF1, all of the SA1 molecules were associated with telomeric DNA and bound to TRF1 (Supplementary Figure S10B). After binding to DNA, SA1 molecules diffused

along the DNA, until captured by a TRF1 molecule, which was typically part of a TRF1 dimer. Meanwhile, in the scenario of an absence of heterodimerization between TRF1 and SA1, only 18% of SA1 was bound to DNA. Importantly, the results were identical at time steps of ∼1, 2 and 4 ps. Thus, the simulations are robust and consistent with the experimental data (Figure 5) showing that the interaction with TRF1 strongly enhances SA1 binding specificity to telomeric sequences. We note that the protein–DNA interactions are dynamic in the sense that SA1 recruitment also influences TRF1 binding affinity, although the net effect is relatively small due to the excess of TRF1 in the current MD simulation models.

DISCUSSION

Cohesin rings do not play a major role in sister telomere cohesion (23). Instead, this role is taken over by the cohesin subunit-SA1 and shelterin proteins. Shelterin proteins normally protect telomeres from DNA damage responses. However, their role in sister telomere cohesion is unclear. Here, we used single-molecule imaging to shed new light on how SA1 achieves telomeric DNA binding specificity, and how TRF1 modulates SA1 DNA binding dynamics. These results demonstrated that SA1 and TRF1 function together in binding to telomeric DNA and promoting DNA–DNA pairing.

Monte Carlo simulations suggest a two-state model for SA1 DNA binding

SA1 and TRF1 have distinct binding patterns along the chromosomes. *In vivo*, TRF1 is found at telomeres (48). This property derives from the high propensity of TRF1
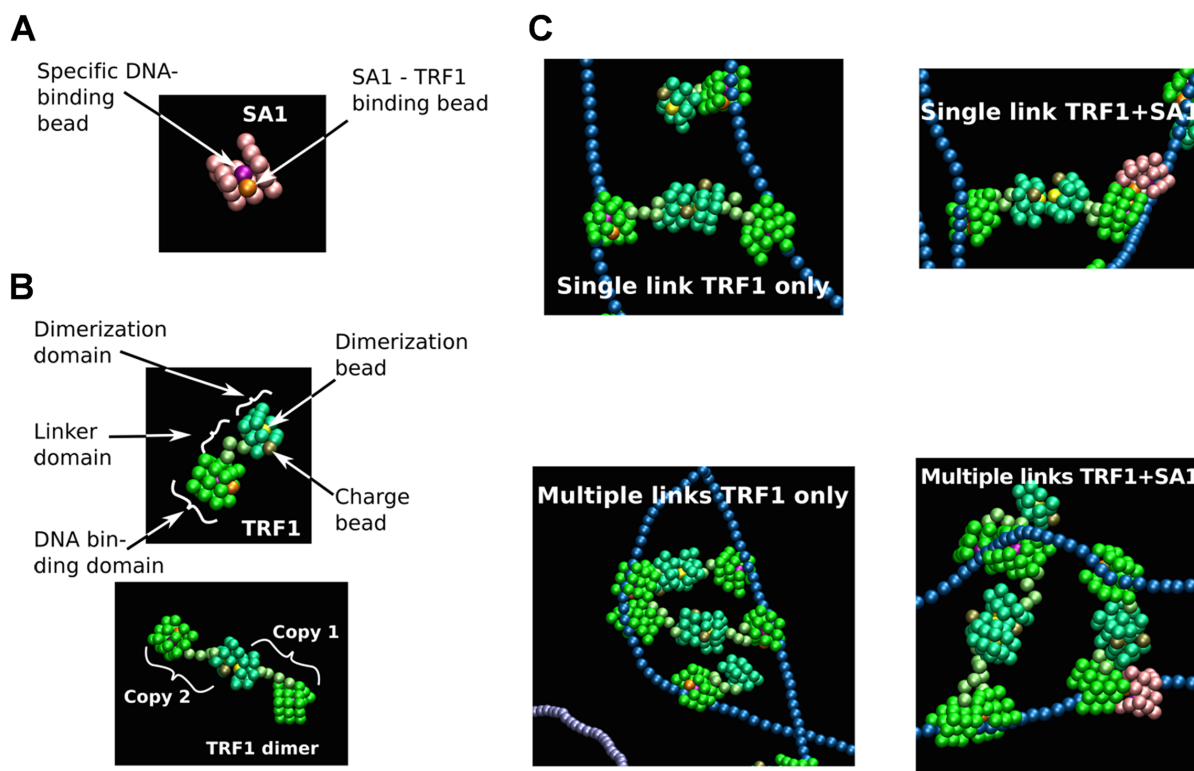
Figure 7. MD simulations of TRF1 and SA1 DNA binding. (**A** and **B**) Coarse-grained structural models for SA1 (**A**) and TRF1 (**B**) used in the simulations. (**C**) TRF1 dimer mediated DNA–DNA pairing in the absence (left panels) or presence of interactions with SA1 (right panels). Examples of zoomed regions from MD simulations show single (top panels) and multiple TRF1-mediated DNA–DNA pairing (bottom panels). Overview pictures from MD simulations of SA1 alone and SA1 + TRF1 are shown in Supplementary Figure S10.

to remain within telomeric regions due to a rougher diffusion energy landscape within these regions compared to genomic sequences (29). In contrast, SA1 has wider roles *in vivo* exemplified by its distribution along chromosome arms (49). Consistent with the roles of SA1 *in vivo*, in this study we found that SA1 diffuses through both telomeric and non-telomeric regions. The diffusion constant of SA1-QDs on T270 tightropes (~ 0.04–0.11 μm^2/s) was comparable with QD-labeled DNA repair proteins including Mlh (0.137 μm^2/s), Mlh1-Pms1 (0.02 – 0.99 μm^2/s) and MutS (0.036 μm^2/s) (50). Based on the Stokes-Einstein relation, the diffusion constant of free SA1 was estimated to be $\sim$0.22 μm^2/s (using the hydrodynamic radius of SAv-QDs: 10.5 nm; and the dimension of SA1 ortholog, yeast Scc3: radius at 6.2 nm) (51–53).

Furthermore, the alternating telomeric and non-telomeric DNA sequences on DNA tightropes allow us to pinpoint specific DNA binding events by correlating the distances between repeated transient DNA binding dynamics with specific DNA sequences. Importantly, for SA1 on T270, we observed defined distances between slow diffusion events consistent with spacing between telomeric regions. These results demonstrate that SA1 diffuses more slowly over telomeric sequences. In addition, on T270 SA1 diffusion shows alpha factors <1, suggesting that SA1 pauses amid free diffusion on DNA. These slow diffusion events are not due to the hydrodynamic drag on QDs and the flexible linker between SA1 and QDs. Using

dissipative particle dynamics simulations, we found that the linker extension was independent of the nanoparticle size and under no circumstances did a nanoparticle tag lead to pausing (Riehn, R., unpublished results). To provide a mechanistic basis for the observed slow diffusion at telomeric sequences, we applied Monte Carlo simulations and modeled SA1 existing in one of two DNA binding states: (i) statically bound (recognition or reading) mode; (ii) freely diffusing (search) mode (Supplementary Methods and Supplementary Figure S11). We assigned less frequent pausing (8%) on non-telomeric DNA for SA1. As SA1 passes into a telomeric region the equilibrium is shifted toward pausing with a 80% probability of entering the paused state. By shifting the equilibrium between these two states we were able to reproduce the diffusive behavior of SA1 with kymographs displaying periods of slow diffusion that coincide with the positions of the telomeric regions (Supplementary Figure S11). The strong qualitative correlation between results from Monte Carlo simulations and single-molecule fluorescence imaging suggests that the two-state model is a plausible mechanism for the observed fast and slow diffusion events on telomeric DNA. Based on these Monte Carlo simulations, an important prediction is that DNA sequence dependent SA1–DNA interaction energy landscape will determine the statistical probability of SA1 being in the sub-diffusive/pausing state. Future experiments need to be carried out to test the SA1–DNA

interaction energy landscape involving high frequency SA1 binding sites *in vivo* (49).

SA1 N-terminal AT-hook domain has dual roles in both specific and non-specific DNA binding

The AT-hook is a small DNA binding motif that has been identified in proteins that play important roles in modulating chromatin structure or functioning as transcription factors (42). The nuclear magnetic resonance structure of an archetypal AT-hook protein HMG-I(Y) reveals that the AT-hook forms a C-shaped structure with the concave surface inserted into the DNA minor groove (54). These non-specific interactions include hydrogen bonds or electrostatic interactions with the DNA phosphate groups. Similar to full length SA1, a higher percentage of SA1-N displays long slow diffusion events on T270 DNA compared to genomic DNA. These results indicate that the slow diffusion events displayed by full length SA1 are mediated at least partly through its N-terminal domain. Our results from using SA1 R37A R39A suggest that, similar to *Lac* repressor, the AT-hook motif in SA1 plays dual roles in non-specific DNA binding as well as in mediating pausing events on DNA for achieving specific DNA binding. For *Lac* repressor, the same set of residues involved in the highly specific DNA binding mode can shift and twist to participate in non-specific DNA binding (55). Our results are also consistent with the notion that thermally driven conformational fluctuations in the DNA binding domains are effectively coupled to the 1D diffusion-mediated target sequence search (56). It has been suggested that there are at least two different conformations of DNA binding domains. A DNA binding domain less ordered in structure enables the fast-diffusing state, while more ordered in structure facilitates recognition of specific DNA binding sites. Furthermore, the function of the AT-hook domain in SA1 is reminiscent of the key 'wedge residue' of Fpg, Nei and Nth DNA glycosylases, which modulates the diffusive behavior of these proteins in searching for DNA lesions (31). A two-state search model has also been proposed for the transcription activator-like effector proteins (57). Future experiments could further investigate whether the two-state (searching and recognition) model is universal for other DNA binding proteins containing the AT-hook motif.

TRF1 confines the diffusion of SA1 within telomeric regions

As a result of the fast alternation between static and free diffusion, SA1 alone can diffuse across multiple telomeric and non-telomeric regions and only temporarily slows down at telomeric sequences. This study provides the experimental evidence for how TRF1 makes SA1 a dedicated telomere binding protein. The observation that TRF1 tethers SA1 at telomeric DNA regions and reduces its probability of entering into non-telomeric DNA regions offers a mechanism by which SA1 can switch from the role of a protein functioning along chromosome arms to one specific to telomeres.

Consistent with previous results (43), we observed TRF1-mediated DNA–DNA pairing in our AFM images. Interestingly, we also found that the addition of SA1 significantly increased the DNA–DNA pairing tract length, as compared

to TRF1 alone. This enhancement depends on SA1 DNA binding. SA1 R37A R39A with diminished DNA binding affinity failed to enhance TRF1-mediated DNA–DNA pairing. Under our imaging conditions (6.7 nM DNA, 30 nM TRF1 and 50 nM SA1), while TRF1 molecules formed closely spaced molecules over the DNA–DNA pairing region, SA1 sparsely decorated TRF1 protein tracts at random positions. It is worth noting that the protein concentrations used in our single-molecule experiments are comparable with estimated TRF1 concentration *in vivo* (58). Coarse-grained MD simulations suggest a model where TRF1 stabilizes SA1 at telomeric sequences and enhances SA1 telomeric DNA binding specificity. Due to their combined DNA binding energy, SA1–TRF1 complexes become more stable than either TRF1 or SA1 alone on telomeric DNA. One mechanism of SA1 action would be to enhanceTRF1 dimer-DNA linkages contributing to the stability and therefore the increase in the length of the DNA–DNA pairing region. Future studies are needed to understand how TIN2 modulates SA1–TRF1–DNA structures and sister telomere cohesion in the context of heterochromatin protein 1γ (HP1γ) and nucleosomes (24,59).

SA1 DNA binding in the context of the core cohesin complex

Cohesin-SA1 and SA2 subunits play different roles in sister chromatid cohesion, DNA repair and transcription regulation (25,60). SA1 deletion causes embryonic lethality (49), demonstrating that SA2 cannot replace the function of SA1. Besides its function at telomeres, SA1 is enriched at promoters and CTCF binding sites. However, by itself, SA1 does not display specificity for CTCF consensus sequences. These results suggest that SA1 localizes at CTCF binding sites through protein–protein interactions. SA1 also displays slow diffusion events on genomic DNA, albeit with shorter dwell times and lower frequencies than on the T270 DNA substrate. This raises the possibility that, much like at telomere sequences, frequent pausing of SA1 at AT-rich promoters can lead to targeting of the core cohesin complexes to these regions. A longer dwell time of SA1 at AT-rich sequences in its recognition (reading) mode could permit the assembly of specific structures to carry out unique functions across the genome. Therefore, we propose a model in which SA1 is the 'DNA sequence guide' (using its AT-hook motif) for the core cohesin complex. It directs the loading of the core cohesin complexes at specific sequences along the genome. Finally, these results support a revised model for cohesin assembly that requires both 1D searching on DNA and DNA sequence specific binding by SA1.

SUPPLEMENTARY DATA

Supplementary Data are available at NAR Online.

REFERENCES

1. Michaelis,C., Ciosk,R. and Nasmyth,K. (1997) Cohesins: chromosomal proteins that prevent premature separation of sister chromatids. *Cell*, **91**, 35–45.
2. Uhlmann,F. and Nasmyth,K. (1998) Cohesion between sister chromatids must be established during DNA replication. *Curr. Biol.*, **8**, 1095–1101.
3. Remeseiro,S. and Losada,A. (2013) Cohesin, a chromatin engagement ring. *Curr. Opin. Cell Biol.*, **25**, 63–71.
4. Skibbens,R.V. (2010) Buck the establishment: reinventing sister chromatid cohesion. *Trends Cell Biol.*, **20**, 507–513.
5. Bose,T. and Gerton,J.L. (2010) Cohesinopathies, gene expression, and chromatin organization. *J. Cell Biol.*, **189**, 201–210.
6. Nasmyth,K. and Haering,C.H. (2009) Cohesin: its roles and mechanisms. *Annu. Rev. Genet.*, **43**, 525–558.
7. Wendt,K.S., Yoshida,K., Itoh,T., Bando,M., Koch,B., Schirghuber,E., Tsutsumi,S., Nagae,G., Ishihara,K., Mishiro,T. *et al.* (2008) Cohesin mediates transcriptional insulation by CCCTC-binding factor. *Nature*, **451**, 796–801.
8. Blackburn,E.H. (2005) Telomeres and telomerase: their mechanisms of action and the effects of altering their functions. *FEBS Lett.*, **579**, 859–862.
9. Palm,W. and de Lange,T. (2008) How shelterin protects mammalian telomeres. *Annu. Rev. Genet.*, **42**, 301–334.
10. Holohan,B., Wright,W.E. and Shay,J.W. (2014) Cell biology of disease: telomeropathies: an emerging spectrum disorder. *J. Cell Biol.*, **205**, 289–299.
11. Lin,J., Kaur,P., Countryman,P., Opresko,P.L. and Wang,H. (2014) Unraveling secrets of telomeres: one molecule at a time. *DNA Rep.*, **20**, 142–153.
12. Wright,W.E., Tesmer,V.M., Huffman,K.E., Levene,S.D. and Shay,J.W. (1997) Normal human chromosomes have long G-rich telomeric overhangs at one end. *Genes Dev.*, **11**, 2801–2809.
13. Cech,T.R. (2004) Beginning to understand the end of the chromosome. *Cell*, **116**, 273–279.
14. Songyang,Z. and Liu,D. (2006) Inside the mammalian telomere interactome: regulation and regulatory activities of telomeres. *Crit. Rev. Eukaryot. Gene Expr.*, **16**, 103–118.
15. Verdun,R.E. and Karlseder,J. (2007) Replication and protection of telomeres. *Nature*, **447**, 924–931.
16. Giraud-Panis,M.J., Pisano,S., Poulet,A., Le Du,M.H. and Gilson,E. (2010) Structural identity of telomeric complexes. *FEBS Lett.*, **584**, 3785–3799.
17. Lewis,K.A. and Wuttke,D.S. (2012) Telomerase and telomere-associated proteins: structural insights into mechanism and evolution. *Structure*, **20**, 28–39.
18. Gunes,C. and Rudolph,K.L. (2013) The role of telomeres in stem cells and cancer. *Cell*, **152**, 390–393.
19. Lormand,J.D., Buncher,N., Murphy,C.T., Kaur,P., Lee,M.Y., Burgers,P., Wang,H., Kunkel,T.A. and Opresko,P.L. (2013) DNA polymerase delta stalls on telomeric lagging strand templates independently from G-quadruplex formation. *Nucleic Acids Res.*, **41**, 10323–10333.
20. Sfeir,A., Kosiyatrakul,S.T., Hockemeyer,D., MacRae,S.L., Karlseder,J., Schildkraut,C.L. and de Lange,T. (2009) Mammalian telomeres resemble fragile sites and require TRF1 for efficient replication. *Cell*, **138**, 90–103.
21. Tittel-Elmer,M., Lengronne,A., Davidson,M.B., Bacal,J., Francois,P., Hohl,M., Petrini,J.H., Pasero,P. and Cobb,J.A. (2012) Cohesin association to replication sites depends on rad50 and promotes fork restart. *Mol. Cell*, **48**, 98–108.
22. Canudas,S. and Smith,S. (2009) Differential regulation of telomere and centromere cohesion by the Scc3 homologues SA1 and SA2, respectively, in human cells. *J. Cell Biol.*, **187**, 165–173.
23. Bisht,K.K., Daniloski,Z. and Smith,S. (2013) SA1 binds directly to DNA through its unique AT-hook to promote sister chromatid cohesion at telomeres. *J. Cell Sci.*, **126**, 3493–3503.
24. Canudas,S., Houghtaling,B.R., Kim,J.Y., Dynek,J.N., Chang,W.G. and Smith,S. (2007) Protein requirements for sister telomere association in human cells. *EMBO J.*, **26**, 4867–4878.
25. Cuadrado,A., Remeseiro,S., Gomez-Lopez,G., Pisano,D.G. and Losada,A. (2012) The specific contributions of cohesin-SA1 to cohesion and gene expression: implications for cancer and development. *Cell Cycle*, **11**, 2233–2238.
26. Haering,C.H. and Jessberger,R. (2012) Cohesin in determining chromosome architecture. *Exp. Cell Res.*, **318**, 1386–1393.
27. Reichel,A., Schaible,D., Al Furoukh,N., Cohen,M., Schreiber,G. and Piehler,J. (2007) Noncovalent, site-specific biotinylation of histidine-tagged proteins. *Anal. Chem.*, **79**, 8590–8600.
28. Aldeek,F., Safi,M., Zhan,N., Palui,G. and Mattoussi,H. (2013) Understanding the self-assembly of proteins onto gold nanoparticles and quantum dots driven by metal-histidine coordination. *ACS Nano*, **7**, 10197–10210.
29. Lin,J., Countryman,P., Buncher,N., Kaur,P., E,L., Zhang,Y., Gibson,G., You,C., Watkins,S.C., Piehler,J. *et al.* (2014) TRF1 and TRF2 use different mechanisms to find telomeric DNA but share a novel mechanism to search for protein partners at telomeres. *Nucleic Acids Res.*, **42**, 2493–2504.
30. Saxton,M.J. and Jacobson,K. (1997) Single-particle tracking: applications to membrane dynamics. *Annu. Rev. Biophys. Biomol. Struct.*, **26**, 373–399.
31. Nelson,S.R., Dunn,A.R., Kathe,S.D., Warshaw,D.M. and Wallace,S.S. (2014) Two glycosylase families diffusively scan DNA using a wedge residue to probe for and identify oxidatively damaged bases. *Proc. Natl. Acad. Sci. U.S.A.*, **111**, E2091–E2099.
32. Berg,O.G., Winter,R.B. and von Hippel,P.H. (1981) Diffusion-driven mechanisms of protein translocation on nucleic acids. 1. Models and theory. *Biochemistry*, **20**, 6929–6948.
33. von Hippel,P.H. and Berg,O.G. (1989) Facilitated target location in biological systems. *J. Biol. Chem.*, **264**, 675–678.
34. Winter,R.B., Berg,O.G. and von Hippel,P.H. (1981) Diffusion-driven mechanisms of protein translocation on nucleic acids. 3. The Escherichia coli lac repressor–operator interaction: kinetic measurements and conclusions. *Biochemistry*, **20**, 6961–6977.
35. Winter,R.B. and von Hippel,P.H. (1981) Diffusion-driven mechanisms of protein translocation on nucleic acids. 2. The Escherichia coli repressor–operator interaction: equilibrium measurements. *Biochemistry*, **20**, 6948–6960.
36. Gorman,J. and Greene,E.C. (2008) Visualizing one-dimensional diffusion of proteins along DNA. *Nat. Struct. Mol. Biol.*, **15**, 768–774.
37. Tafvizi,A., Mirny,L.A. and van Oijen,A.M. (2011) Dancing on DNA: kinetic aspects of search processes on DNA. *Chemphyschem*, **12**, 1481–1489.
38. Dunn,A.R., Kad,N.M., Nelson,S.R., Warshaw,D.M. and Wallace,S.S. (2011) Single Qdot-labeled glycosylase molecules use a wedge amino acid to probe for lesions while scanning along DNA. *Nucleic Acids Res.*, **39**, 7487–7498.
39. Hughes,C.D., Wang,H., Ghodke,H., Simons,M., Towheed,A., Peng,Y., Van Houten,B. and Kad,N.M. (2013) Real-time single-molecule imaging reveals a direct interaction between UvrC and UvrB on DNA tightropes. *Nucleic Acids Res.*, **41**, 4901–4912.
40. Kad,N.M., Wang,H., Kennedy,G.G., Warshaw,D.M. and Van Houten,B. (2010) Collaborative dynamic DNA scanning by nucleotide excision repair proteins investigated by single- molecule imaging of quantum-dot-labeled proteins. *Mol. Cell*, **37**, 702–713.
41. Ghodke,H., Wang,H., Hsieh,C.L., Woldemeskel,S., Watkins,S.C., Rapić-Otrin,V. and Van Houten,B. (2014) Single-molecule analysis reveals human UV-damaged DNA-binding protein (UV-DDB) dimerizes on DNA via multiple kinetic intermediates. *Proc. Natl. Acad. Sci. U.S.A.*, **111**, E1862–E1871.
42. Aravind,L. and Landsman,D. (1998) AT-hook motifs identified in a wide variety of DNA-binding proteins. *Nucleic Acids Res.*, **26**, 4413–4421.
43. Griffith,J., Bianchi,A. and de Lange,T. (1998) TRF1 promotes parallel pairing of telomeric tracts in vitro. *J. Mol. Biol.*, **278**, 79–88.

44. Anderson,J.A., Lorenz,C.D. and Travesset,A. (2008) General purpose molecular dynamics simulations fully implemented on graphics processing units. *J. Comput. Phys.*, **227**, 5342–5359.

45. Bianchi,A., Stansel,R.M., Fairall,L., Griffith,J.D., Rhodes,D. and de Lange,T. (1999) TRF1 binds a bipartite telomeric site with extreme spatial flexibility. *EMBO J.*, **18**, 5735–5744.

46. Opresko,P.L., Fan,J., Danzy,S., Wilson,D.M. 3rd and Bohr,V.A. (2005) Oxidative damage in telomeric DNA disrupts recognition by TRF1 and TRF2. *Nucleic Acids Res.*, **33**, 1230–1239.

47. Parikh,D., Fouquerel,E., Murphy,C.T., Wang,H. and Opresko,P.L. (2015) Telomeres are partly shielded from ultraviolet-induced damage and proficient for nucleotide excision repair of photoproducts. *Nat. Commun.*, **6**, 8214.

48. Garrobo,I., Marion,R.M., Dominguez,O., Pisano,D.G. and Blasco,M.A. (2014) Genome-wide analysis of in vivo TRF1 binding to chromatin restricts its location exclusively to telomeric repeats. *Cell Cycle*, **13**, 3742–3749.

49. Remeseiro,S., Cuadrado,A., Gomez-Lopez,G., Pisano,D.G. and Losada,A. (2012) A unique role of cohesin-SA1 in gene regulation and development. *EMBO J.*, **31**, 2090–2102.

50. Kad,N.M. and Van Houten,B. (2012) Dynamics of lesion processing by bacterial nucleotide excision repair proteins. *Prog. Mol. Biol. Transl. Sci.*, **110**, 1–24.

51. Schurr,J.M. (1979) The one-dimensional diffusion coefficient of proteins absorbed on DNA. Hydrodynamic considerations. *Biophys. Chem.*, **9**, 413–414.

52. Arnspang,E.C., Brewer,J.R. and Lagerholm,B.C. (2012) Multi-color single particle tracking with quantum dots. *PLoS One*, **7**, e48521.

53. Roig,M.B., Lowe,J., Chan,K.L., Beckouet,F., Metson,J. and Nasmyth,K. (2014) Structure and function of cohesin's Scc3/SA regulatory subunit. *FEBS Lett.*, **588**, 3692–3702.

54. Huth,J.R., Bewley,C.A., Nissen,M.S., Evans,J.N., Reeves,R., Gronenborn,A.M. and Clore,G.M. (1997) The solution structure of an HMG-I(Y)-DNA complex defines a new architectural minor groove binding motif. *Nat. Struct. Biol.*, **4**, 657–665.

55. Kalodimos,C.G., Biris,N., Bonvin,A.M., Levandoski,M.M., Guennuegues,M., Boelens,R. and Kaptein,R. (2004) Structure and flexibility adaptation in nonspecific and specific protein-DNA complexes. *Science*, **305**, 386–389.

56. Murugan,R. (2010) Theory of site-specific DNA-protein interactions in the presence of conformational fluctuations of DNA binding domains. *Biophys. J.*, **99**, 353–359.

57. Cuculis,L., Abil,Z., Zhao,H. and Schroeder,C.M. (2015) Direct observation of TALE protein dynamics reveals a two-state search mechanism. *Nat. Commun.*, **6**, 7277.

58. Takai,K.K., Hooper,S., Blackwood,S., Gandhi,R. and de Lange,T. (2010) In vivo stoichiometry of shelterin components. *J. Biol. Chem.*, **285**, 1457–1467.

59. Canudas,S., Houghtaling,B.R., Bhanot,M., Sasa,G., Savage,S.A., Bertuch,A.A. and Smith,S. (2011) A role for heterochromatin protein 1gamma at human telomeres. *Genes Dev.*, **25**, 1807–1819.

60. Peters,J.M. (2012) The many functions of cohesin–different rings to rule them all? *EMBO J.*, **31**, 2061–2063.

SUPPLEMENTARY INFORMATION

For manuscript

Functional interplay between SA1 and TRF1 in telomeric DNA binding and DNA-DNA pairing

Jiangguo Lin[1,2], Preston Countryman[2], Haijiang Chen[3,4], Hai Pan[2], Yanlin Fan[3], Yunyun Jiang[3], Parminder Kaur[2], Wang Miao[5], Gisele Gurgel[6], Changjiang You[7], Jacob Piehler[7], Neil M. Kad[8], Robert Riehn[2], Patricia L. Opresko[9], Susan Smith[10], Yizhi Jane Tao[3], Hong Wang[2,*]

[1]School of Bioscience and Engineering, South China University of Technology, Guangzhou, Guangdong 510006, P. R. China

[2]Physics Department, [6]Biomanufacturing Training and Education Center, North Carolina State University, Raleigh, North Carolina, NC 27695, USA

[3]Department of BioSciences, Rice University, Houston, TX 77005, USA

[4]Institute of Microbiology and College of Life Sciences, Zhejiang University, Hangzhou, Zhejiang, 310058, P. R. China

[5]Department of Neurology, The First Affiliated Hospital of Zhengzhou University, Zhengzhou, Henan, 450014, P. R. China

[7]Division of Biophysics, *Universität Osnabrück*, Barbarstrasse 11, 49076, *Osnabrück*, Germany

[8]School of Biosciences, University of Kent, Canterbury, Kent, CT2 7NJ, United Kingdom

[9]Department of Environmental and Occupational Health, University of Pittsburgh, Pennsylvania 15213, USA

[10]Kimmel Center for Biology and Medicine at the Skirball Institute, Department of Pathology, New York University School of Medicine, New York, NY 10016.

This Supplementary Information contains:

Supplementary Methods

Supplementary Figures S1–11

Supplementary Legends for Movies S1–3

Supplementary References

Supplementary Methods

DNA substrates for single-molecule imaging

pSP73 vector (Promega) derived pSXneo(T2AG3) plasmid DNA containing 270 TTAGGG repeats (T270) was purchased from Addgene and purified from Stbl2 cells (Invitrogen) to retain stable telomeric DNA lengths (62). To generate DNA fragments containing TTAGGG repeats for AFM imaging, the restriction digestion of T270 DNA (10 µg) was carried out at 37 °C for 4 hr using *HpaI* (130 U) in Buffer 4 (New England BioLabs). Final DNA substrate purification was done using a PCR DNA Purification Kit (Qiagen). To generate the DNA substrate containing centromeric sequences, first, a 1.7 kb PCR product with human X-linked alpha-satellite sequences was generated using the forward primer (5' GCC GAT TCA TTA ATG CAG GTT AAC AAA GGC TTT CAG GCT TTT CCA CCA 3'), reverse primer (5'AAT TTC GAT AAG CCA GGT TAA CAA GTG GCT ATT TAG CGG CTG GA 3'), and genomic DNA purified from MDA-MB-231 breast cancer cells as the template. The PCR product was gel purified and subsequently cloned into the pSP73 vector (Promega) digested with HpaI. In order to generate longer DNA substrates for the DNA tightrope assay, linearized DNA substrates were ligated using the Quick Ligation™ Kit (New England BioLabs) at room temperature for 30 min. Ligated DNA samples were then purified using phenol-chloroform extraction.

Protein purification

The full length WT SA1 and SA1 R37A R39A mutant (1258 AA) containing a N-terminal 3X Flag tag (DYKDHDGDY KDHDIDYKDD DDK) was overexpressed using a baculoviruse system and purified using the anti-Flag M2 column (GenScript). To purify the 6xHis tagged SA1 (His-SA1), ~2 x 10^8 Sf21 cells were transfected with baculoviruses overexpressing His-SA1 and harvested 48 hr post-infection. Cell pellets were re-suspended in 10 ml of Ni-NTA buffer A (50 mM Tris-HCl, pH 7.5, 300 mM NaCl, 20 mM imidazole, 10% glycerol, 0.1 mM PMSF) and lysed by sonication. Supernatants from the lysates were collected by 35,000 g x 40 min centrifugation and loaded onto 0.2 ml of pre-equilibrated Ni-NTA resin (Qiagen). The supernatant was then constantly mixed with the resin at 4°C for 1 hr. The resin was collected by 1,000 g x 3 min centrifugation and the supernatant (flow through) was removed. The resin was then washed with 5 ml of Ni-NTA Buffer A. The proteins bound to the Ni-NTA agarose were eluted by Ni-NTA buffer B (50 mM Tris-HCl, pH 7.5, 300 mM NaCl, 250 mM imidazole, 10% glycerol, 0.1 mM PMSF). The concentration of the purified protein was determined by the Bradford protein assay using BSA as the protein concentration standard. SA1 was more than 90% pure based on SDS-PAGE analysis. The His$_6$-tagged single-chain antibody fragment (37 KDa) was overexpressed in *E. coli* and purified using a Ni-NTA agarose column (Qiagen) according to protocols specified by the manufacture.

Fluorescence anisotropy

The telomeric and non-telomeric DNA substrates were made by annealing 5' Alexa488 labeled top and unlabeled complementary stands using the following oligos:

Alexa-Tel7-top:

5'CTGGATCCGTAC**TTAGGGTTAGGGTTAGGGTTAGGGTTAGGGTTAGGGTTAGGG**ACAAGAATTCGA3'

Tel7-com:

5'TCGAATTCTTGT**CCCTAACCCTAACCCTAACCCTAACCCTAACCCTAACCCTAA**GTACGGATCCAG3'

Scram-top:

5'CTGGATCCGTACAGTGTAAGGGTGAGTGGTTGGGTGTGTGGGTGTTGATGTAGAACAAGAATTCGA3'

Scram-com:

5' TCGAATTCTTGTTCTACATCAACACCCACACACCCAACCACTCACCCTTACACTGTACGGATCCAG3'

Flag-tagged full length SA1 was concentrated 10-fold from 0.110 mg/ml (stock concentration) to 1.1 mg/ml and dialyzed in the DNA binding buffer [20 mM Hepes (pH 7.5), 0.1 mM MgCl$_2$, 0.5 mM DTT, 100 mM KCl] to remove the glycerol in the storage buffer. SA1 was then titrated into the binding solution containing DNA (0.2 nM) until the millipolarization (mP) stabilized. The data were plotted and analyzed by using the equation P = {(P$_{bound}$ −P$_{free}$)[protein]/(K_d + [protein])} + P$_{free}$, where P is the polarization measured at a given total protein concentration, P$_{free}$ is the initial polarization of Alexa488-labeled DNA without protein bound, P$_{bound}$ is the maximum polarization of DNA when all DNA molecules are bound by proteins, and [protein] is the protein concentration. The free and total protein concentrations were assumed to be equal since the K_d was at least 10-fold higher than the concentration of Alex488-labeled DNA. The binding curves were fitted by the nonlinear least-squares regression analysis assuming a bimolecular model of pseudo first order such that the K_d values represent the protein concentrations at which half of the DNA substrates are in the bound-state.

Electrophoresis mobility shift assays (EMSAs)

The telomeric DNA substrate used for EMSAs was constructed by annealing a 5' Alexa488 labeled oligo (5'TTA GGG TTAGGG TTAGGG ATG TCC AGC AAG CCA GAA TTC GGC AGC GTA3') with a second unlabeled oligo containing its complementary sequences. TRF1 and SA1 DNA binding reactions were carried out in a buffer containing 20 mM Hepes (pH 7.9), 150 mM KCl, 1 mM MgCl, 0.5 mM DTT, 0.25% NP-40, and 5% glycerol with DNA substrate and protein concentrations indicated in the figure legends (Figure 5A). The reactions were run by gel electrophoresis on a 5% 29:1 (bisacrylamide:acrylamide) native gel at 4°C and 150 V for about 40 min in 1X TBE buffer. The gel was visualized using a Typhoon FLA 7000 Phosphorimager. The percentages of unbound and bound DNA substrate were quantified using ImageQuant software.

Coarse-grained molecular dynamics simulations

We used the molecular dynamics package HOOMD-blue to explore the probable pathway that leads to protein-mediated DNA-DNA pairing under the action of a coarse-grained, simplified functional model of SA1 and TRF1. All molecules are made of 1 nm-wide beads. Bonded interactions within DNA and the protein are represented through a harmonic potential with spring stiffness of 330 k_BT/nm^2. Mutual steric exclusion between all pairs of particles is ensured by truncated shifted Lennard-Jones potentials. DNA is modeled as a chain of bonded beads with harmonic angle potentials. Non-bonded DNA segment pairs interact through a screened Coulomb potential, which raises the persistence length to 50 nm (63). Protein domains mainly consist of "inert" beads that are present only to establish steric structures containing the DNA binding (Myb) domain, linker, dimerization domain for TRF1, and only a DNA binding domain for SA1.

Specific attractive interactions were added to this model by adding specific beads with additional Lennar-Jones interaction terms. Specifically, those interactions are between

1) A bead within the groove of either SA1 or the DNA-binding domain of TRF1 and DNA.
2) A bead at the center of the TRF1 dimerization domain and the corresponding bead at the center of another TRF1 dimerization domain.
3) A bead at the side of SA1 (along the DNA binding groove) and a bead at the side of the DNA-binding domain of TRF1 (in the same location as the bead on SA1).

The model is integrated using a Langevin integrator.

Time steps were ~1, 2, or 4 ps, and the total time scale of the simulation was ~ 3 ms. Results were identical with different time steps. Because DNA was confined to a small simulation box, the effective concentration of DNA (400 mg/l, 6.7×10^{-4} mol/l of bp) was rather high, requiring a similarly high concentration of TRF1 (1.9×10^{-5} mol/l) and SA1 (1.9×10^{-6} mol/l) to create similar ratios of protein to DNA compared to experimental conditions.

Monte Carlo Simulations of protein diffusion on DNA

To determine if the observed slowing of SA1 diffusion at telomere sequences could be due to pausing, Monte Carlo simulations were performed using MATLAB. The model is based on the assumption that protein molecules exist in two states (free diffusing and pausing) and the DNA context affects the equilibrium between these states. We created a model DNA strand with 1.6 kb telomeric sequences spaced 3.8 kb apart by non-telomeric DNA. For every simulation cycle the molecule could either take a 10 bp step with a probability of stepping (equal chance for forwards/backwards) or pausing. When the protein molecule was in regions containing non-telomere DNA, a bias was applied towards the probability of stepping of 92%. Upon entering a region defined as containing telomeric DNA, the probability of stepping was reduced to 20%. Pausing durations were randomly selected from an exponential probability distribution. The number of iterations used was 1×10^4. However, because the

duration of pausing advanced the step position, consequently the total number of steps simulated was ~10x greater than the iteration number. The trace shown in Supplementary Figure S11 is highly representative of all the traces simulated.

Supplementary Movie Legends

1. **Supplementary Movie S1.** A full length Flag-SA1-QD complex displaying alternation between slow and fast diffusion on a T270 DNA tightrope. The scale bar is 1 μm.

2. **Supplementary Movie S2.** A SA1-N-QD complex displaying alternation between slow and fast diffusion on a T270 DNA tightrope. The scale bar is 1 μm.

3. **Supplementary Movie S3.** A dual color differentially QD-labeled SA1-TRF1 complex showing subdiffusive motion on a T270 DNA tightrope. The scale bar is 1 μm.

Supplementary References

62. Hanish, J.P., Yanowitz, J.L. and de Lange, T. (1994) Stringent sequence requirements for the formation of human telomeres. *Proceedings of the National Academy of Sciences of the United States of America*, **91**, 8861-8865.

63. Hsieh, C.C., Balducci, A. and Doyle, P.S. (2008) Ionic effects on the equilibrium dynamics of DNA confined in nanoslits. *Nano letters*, **8**, 1683-1688.
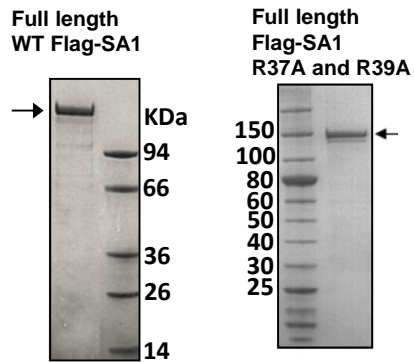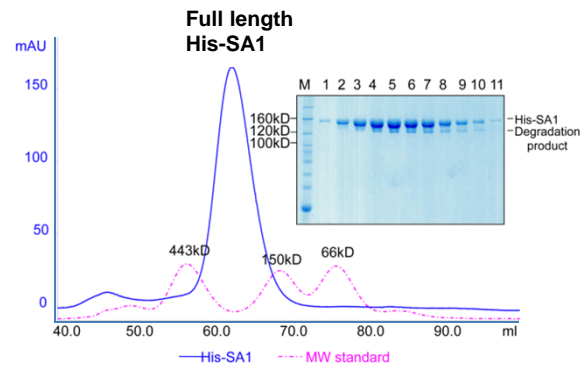
Supplementary Figure S1. Purification of His- and Flag-tagged full length SA1 and characterization of the oligomeric state of SA1 in solution. (**A**) Coomassie blue stained SDS-PAGE gel of Flag-tagged WT SA1 and SA1 R37A R39A mutant (Genscript). (**B**) Evaluation of the oligomeric state of the full length His-SA1 in solution using a gel filtration column. Lanes 1-11, peak fractions from gel filtration.

A

CTCF-WT DNA sequences (CTCF-WT):
5'Cy3/TCCACAATGACATGATGGCCAGCAGAGGGCGCATGGCCCTGGGGACCT3'
Shuffled DNA sequences (CTCF-SH):
5'Cy3/TCCACAATGACATGGCAGCATGGCGTGCGAGAACGGCCCTGGGGACCT3'

B
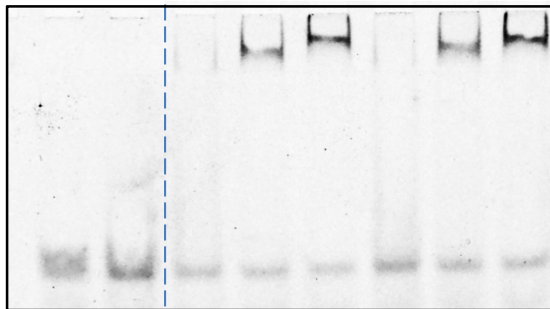
CTCF-SH	+	-	+	+	+	-	-	-
CTCF-WT	-	+	-	-	-	+	+	+
SA1 (nM)	-	-	55	165	330	55	165	330

C
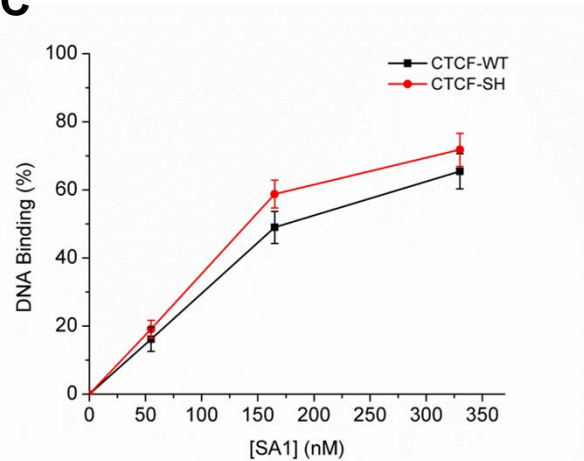
Supplementary Figure S2. SA1 does not specifically bind to consensus CTCF DNA binding sequences. (**A**) The DNA substrate with consensus CTCF DNA binding sequences and control substrate with shuffled sequences used for EMSAs. The sequences from the top strands are shown. (**B**) EMSA of Flag-tagged WT SA1 in the presence of the Cy3-labeled DNA substrates containing consensus CTCF DNA binding sequences or shuffled DNA sequences. The dotted line indicates that the picture is combined from two regions in one gel. (**C**) Quantification of the percentage of DNA binding based on EMSAs. The error bars are standard deviations from two independent experiments.

A

|	Flag-SA1 (%, N = 107)	SA1+TRF1 dual-color (%, N = 101)
Type I	0	0
Type II	0	1.3 ± 1.0
Type III	21.0 ± 7.0	20.3 ± 10.4
Type IV	78.5 ± 7.0	78.4 ± 9.6

B

time 2 min
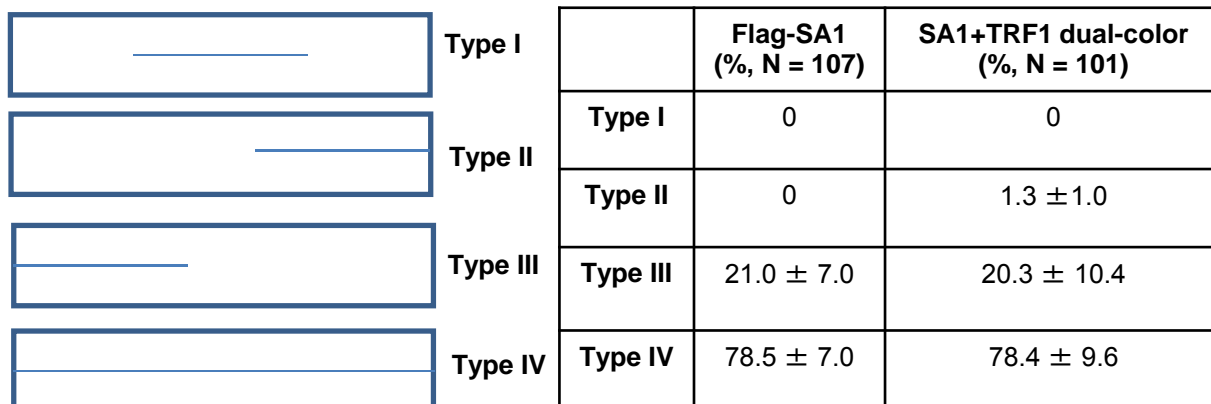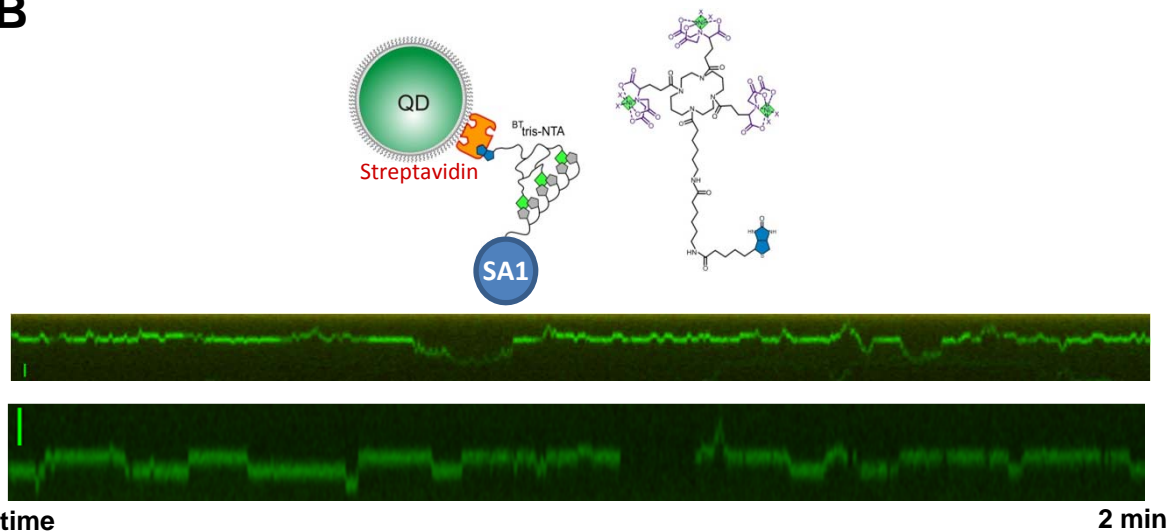
Supplementary Figure S3. Classification of different types of SA1-DNA interactions (A) and QD-labeled His-tagged SA1 on T270 DNA tightropes (B). (**A**) Cartoon drawings of different types of SA1-DNA interactions (left) and statistical analysis of these different types for Flag-SA1 and SA1-TRF1 complexes. Type I: a protein binds and then releases; Type II: a protein binds and doesn't leave; Type III: a protein is bound at the beginning of the movie but releases; Type IV: a protein is bound from the beginning to end of the movie. Reliable attached lifetime measurements could only be obtained from analysis of the Type I interactions, which were not obtained for this study. (**B**) Top panel: conjugating His-tagged SA1 to SAv-QDs was achieved using the biotinylated multivalent chelator tris-nitrilotriacetic acid (BTtris-NTA). Bottom panel: Dynamics of His-SA1-QDs on T270 DNA tightropes. Scale bars (y-axis: 1 μm).

A

50 mM KCl

2 min

B

150 mM KCl

2 min
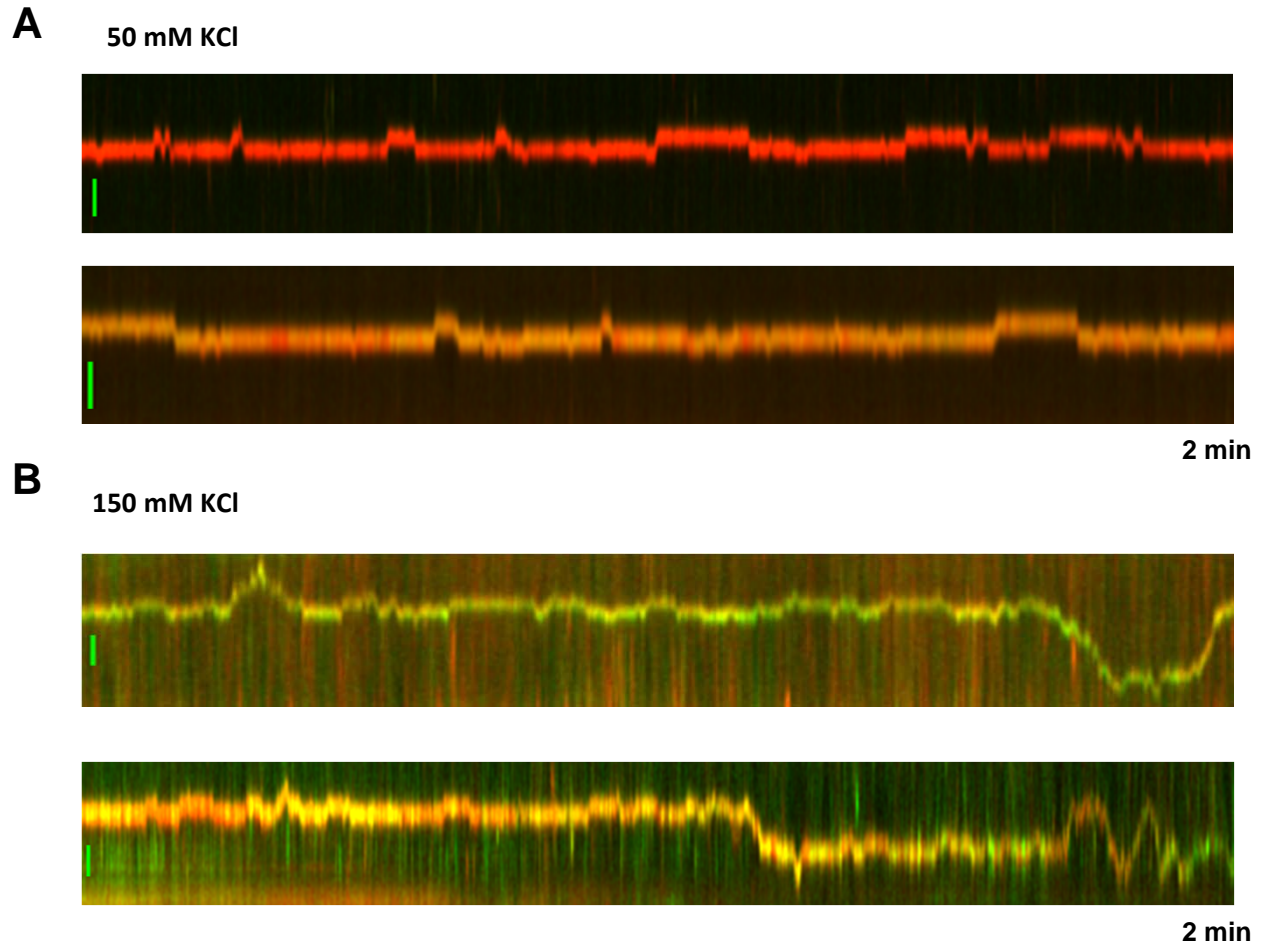
Supplementary Figure S4. The full length Flag-SA1 alternates between fast and slow diffusion at lower (A), and higher (B) salt concentrations. Representative kymographs of Flag-SA1 on T270 DNA tightropes in buffers containing 50 mM KCl (**A**) or 150 mM KCl (**B**). Scale bars (y-axis): 1 μm. Equal molar concentrations of red (655 nm) and green (565 nm) Ab-QDs were used in the SA1 conjugation. All buffers containing additional 20 mM Tris (pH 7.5) and 0.1 mM $MgCl_2$.
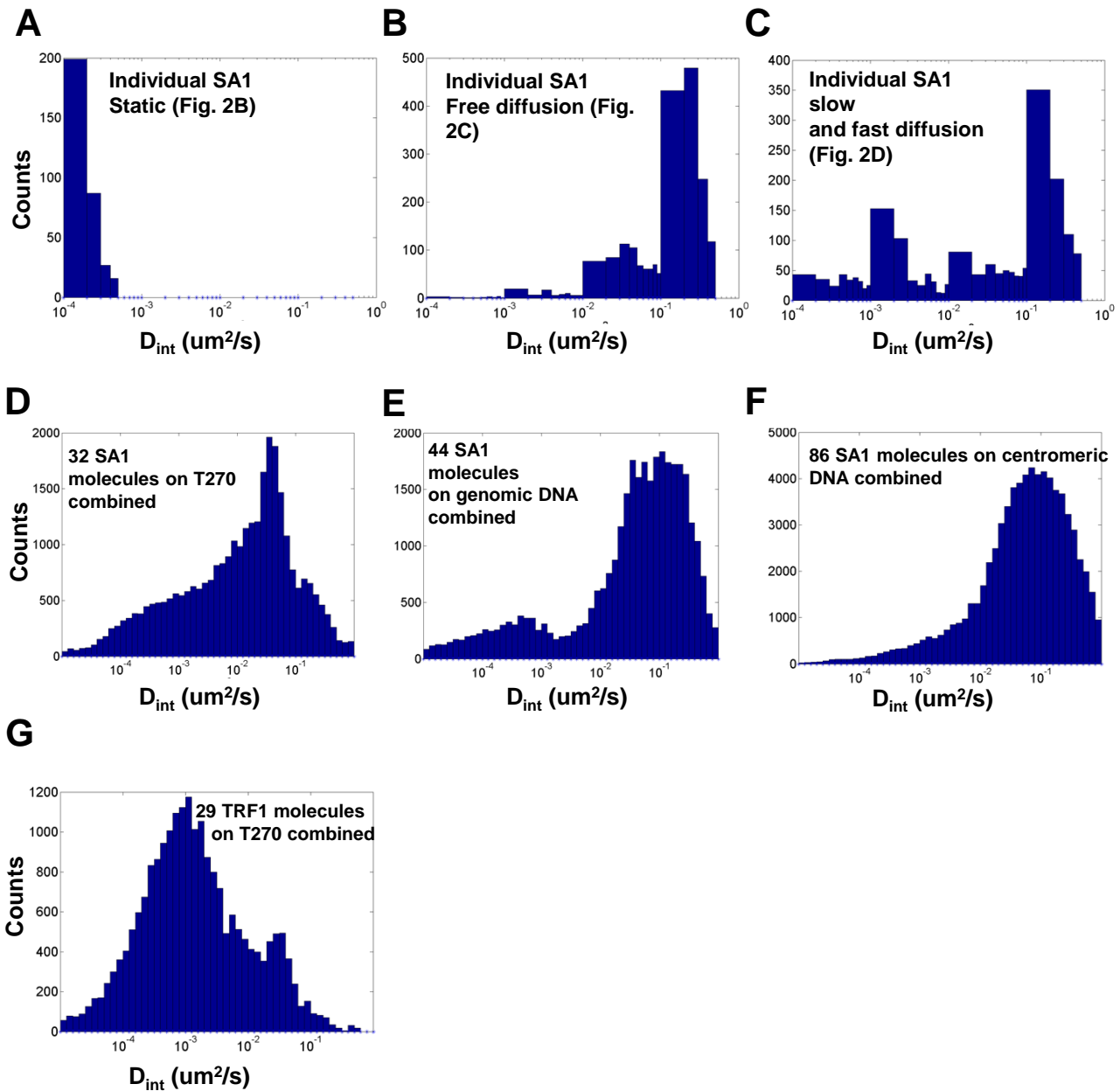
Supplementary Figure S5. Comparison of the distributions of interval based diffusion constants (D_{int}) for SA1 (A-F) and TRF1 (G). (**A**-**C**) Distributions of D_{int} for individual SA1 molecules on T270 DNA tightropes with static (A, kymograph in Fig. 2B), free diffusion (B, kymograph in Fig. 2C), and alternation between fast and slow 1-D diffusion (C, kymograph in Fig. 2D). The SA1 molecules with alternation between fast and slow diffusion show a distinct peak at ~1.0 X10^{-3} µm²/s. (**D**-**F**) Distributions of D_{int} for all mobile SA1 molecules observed on T270 (**D**), genomic (**E**), and centromeric (**F**) DNA tightropes. On T270 DNA, SA1 molecules alternate between fast and slow diffusion with 46% of D_{int} values less than 1X 10^{-2} µm²/s. In comparison, on genomic and centromeric DNA fast diffusion dominates with only 25% and 18% of D_{int} values less than 1X 10^{-2} µm²/s, respectively. (**G**) The distribution of D_{int} for all (N = 29) mobile TRF1 molecules on T270 reported in a previous study (Lin et al., 2014). On T270 DNA, the majority (84%) of the TRF1 D_{int} values is consistent with slow diffusion (less than 1X 10^{-2} µm²/s).
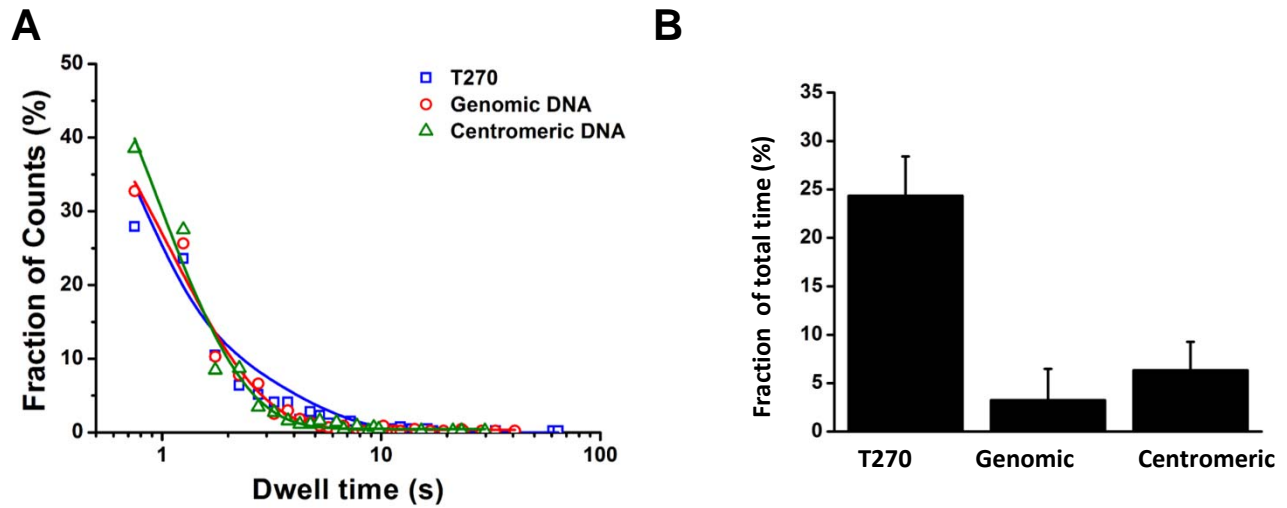
Supplementary Figure S6. Analysis of the dwell time shows distinct DNA binding dynamics by full length WT SA1 on T270 DNA tightropes. (A) Dwell times of individual slow diffusion events on T270 (dwell time: 1.17 s, R^2: 0.97, N = 437), the genomic substrate (dwell time: 0.80 s, R^2: 0.99, N = 437), and the DNA substrate containing centromeric sequences (dwell time: 0.79 s, R^2: 0.97, N = 438). The data sets were fitted with a single exponential decay function. (**B**) SA1 spends a higher percentage of time in the slow diffusion mode out of the total dwell time on T270 DNA (24.4%, N = 18), compared to on genomic (3.2%, N = 8) and centromeric (6.3%, N = 21) DNA substrates. Error bars: SEM.
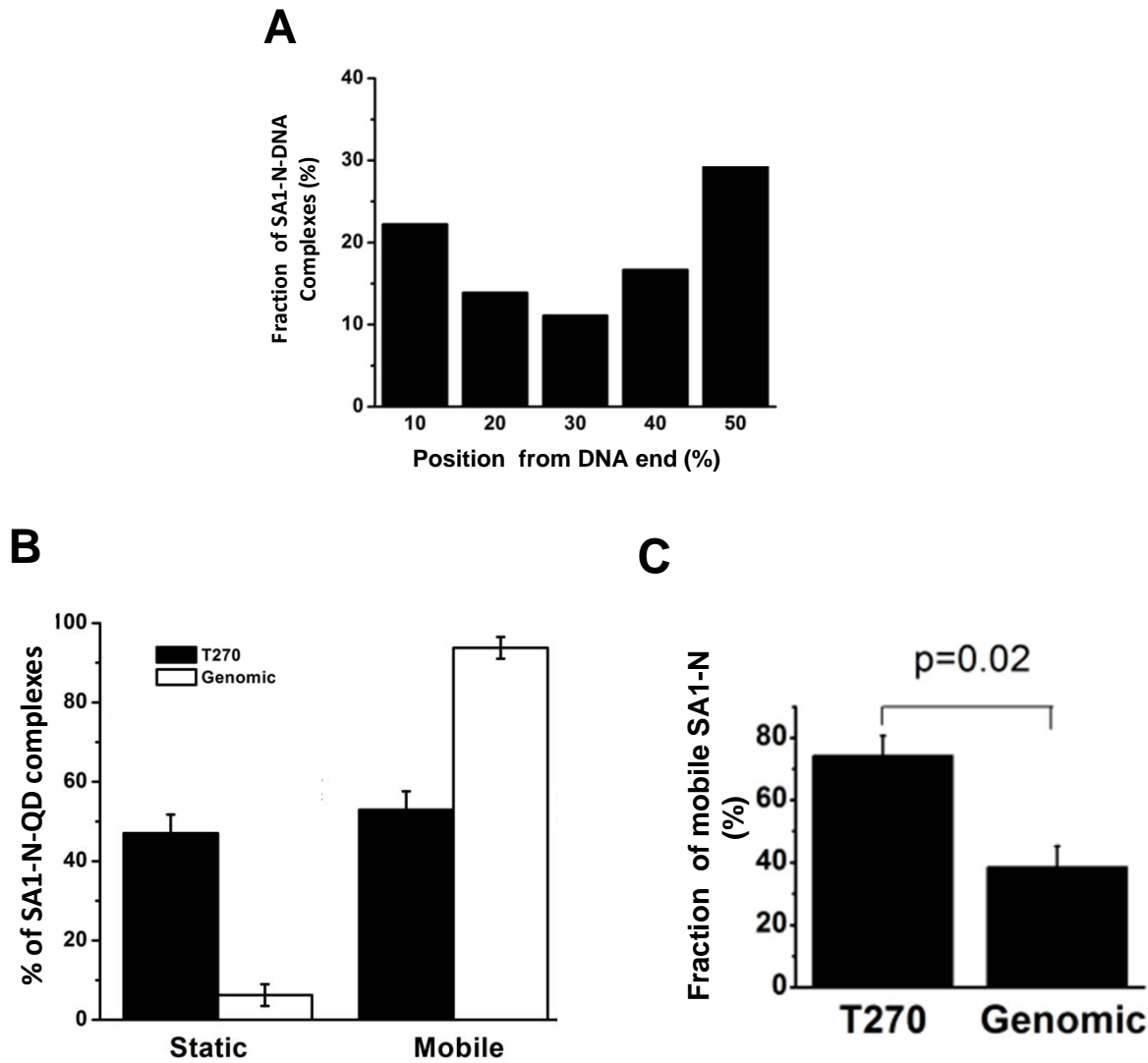
Supplementary Figure S7. The SA1 N-terminal domain (SA1-N) displays alternation between fast and slow diffusion on T270 DNA tightropes. (**A**) The position distribution of SA1-N on T270 DNA based on the analysis of AFM images of SA1-N-T270 complexes. Similar to the full length SA1 (Fig. 1), SA1-N preferentially binds to the telomeric region (35 – 50%) on T270 (N = 36). (**B**) On T270 tightropes, SA1-N displays a higher percentage of static (47.1%) complexes, compared to on genomic DNA (6.2%). (**C**) On T270 tightropes, mobile SA1-N molecules display a higher percentage (74.3%, N = 88) of complexes with slow diffusion events ($D_{in} < 5.0 \times 10^{-3}$ µm^2/s, dwell time > 2.2 s), compared to on genomic DNA (38.6%, N = 103).
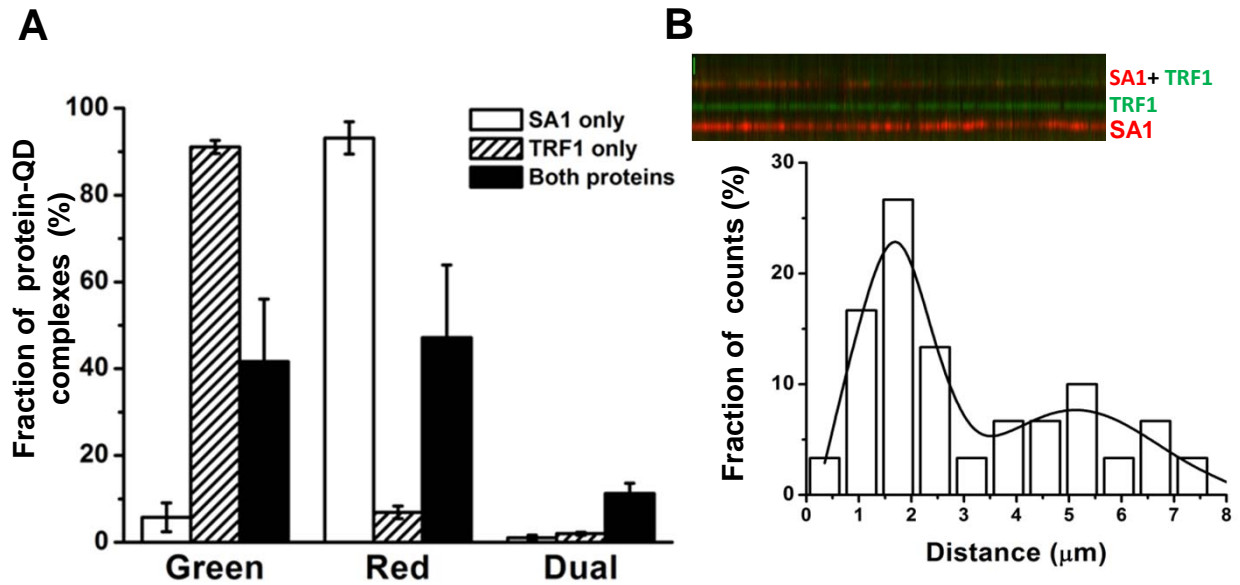
Supplementary Figure S8. Validation of the dual-color-labeling strategy for SA1-TRF1 complexes. (**A**) Formation of dual-color QD-labeled complexes on T270 tightropes depends on the presence of both TRF1 and SA1. In all experiments, ^{BT}tris-NTA, red Ab-QDs, and green SAv-QDs were present in flow cells. The percentages of green, red, and dual-color labeled QD complexes observed in the presence of SA1 only (white bars, N = 190), TRF1 only (striped bars, N = 358), or both TRF1 and SA1 (N = 235) are shown. Error bars: SEM based on at least three independent experiments. The percentage of dual-color QD-labeled complexes on T270 (11.2%) in the presence of both TRF1 and SA1 is 5.6- and 10-fold higher than when only SA1 (2.0%) or TRF1 (1.1%) was present, respectively. (**B**) Dual-color QD-labeled SA1-TRF1 complexes were present at telomeric regions on T270. The distribution of pair-wise distance between green QD-labeled TRF1 (makers for telomeric regions) and dual-color QD-labeled SA1-TRF1 complexes is consistent with the spacing between telomeric regions on T270. The data set (N = 30) was fitted with a double Gaussian function with peaks centered at 1.6 $\pm$ 0.08 µm (distance between two nearest neighbor (TTAGGG)$_{270}$ regions) and 5.1 $\pm$ 0.36 µm. The insert shows a representative kymograph (120 s) used for the distance analysis.
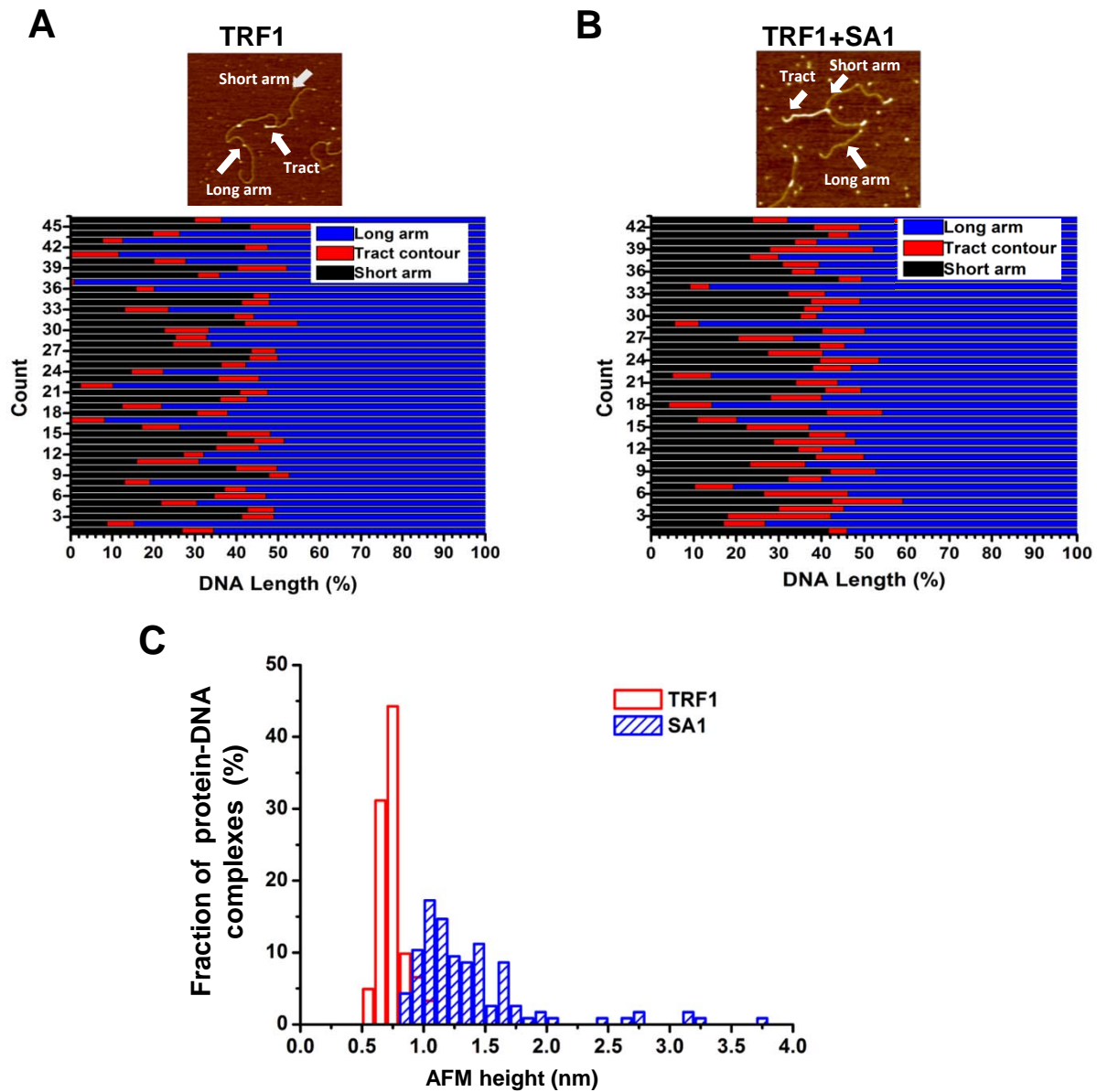
Supplementary Figure S9. Comparison of TRF1 and SA1-TRF1 DNA binding. Protein mediated DNA-DNA pairing tract lengths on T270 DNA in the presence of only TRF1 (**A**) or both SA1 and TRF1 (**B**). (**C**) Comparison of the AFM height of TRF1 and SA1 only on T270 DNA. The AFM height of TRF1 and SA1 on T270 DNA is 0.73 (±0.1, mean ±SD, N = 61) nm, and 1.39 (±0.5, mean ±SD, N = 116) nm, respectively.
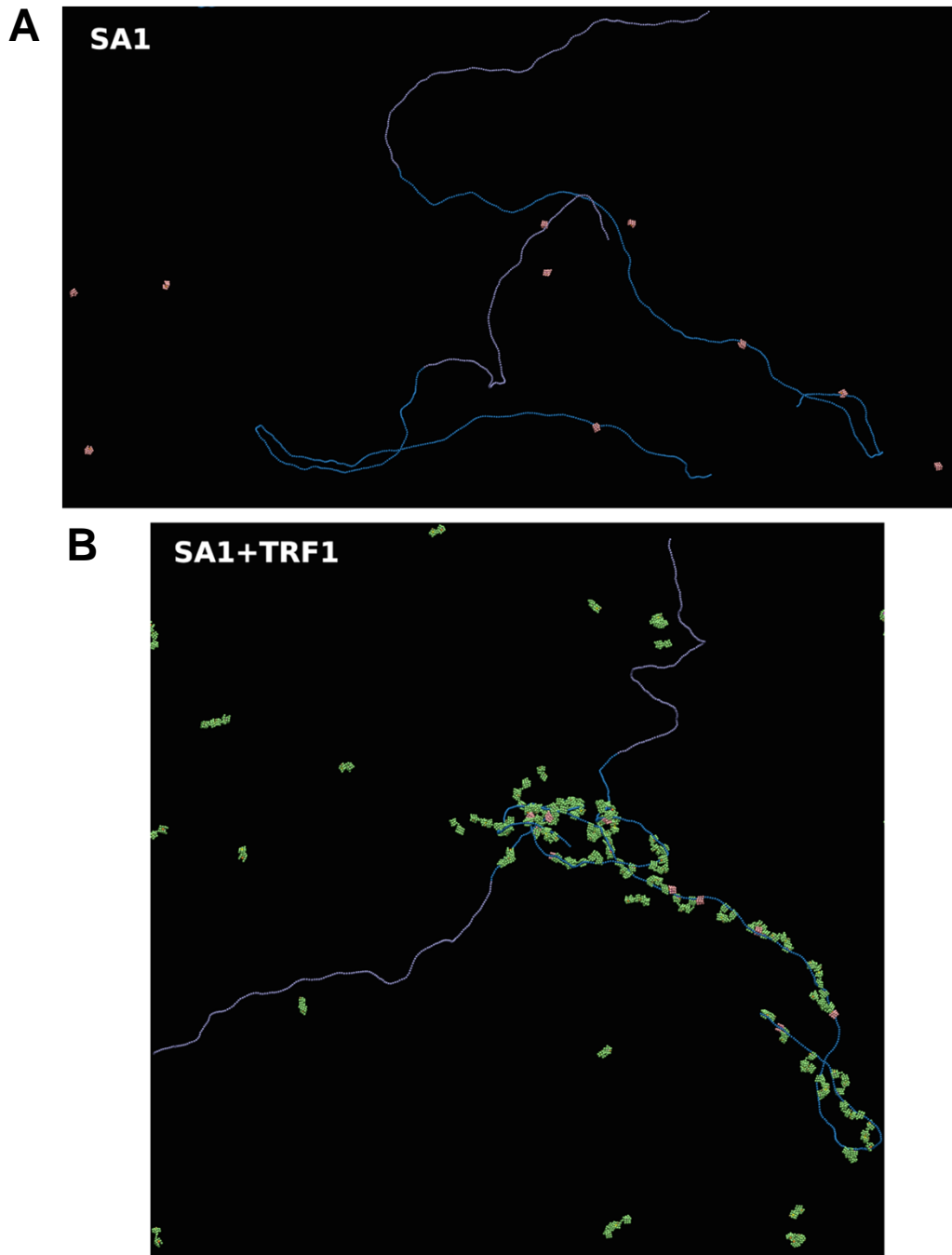
Supplementary Figure S10. Overview of the MD simulations of SA1 (A) and SA1-TRF1 (B) DNA binding. Regions representing genomic (600 bp) and telomeric DNA (1200 bp) DNA are shown in purple and dark blue, respectively. The SA1 and TRF1 models are shown in Fig. 7.
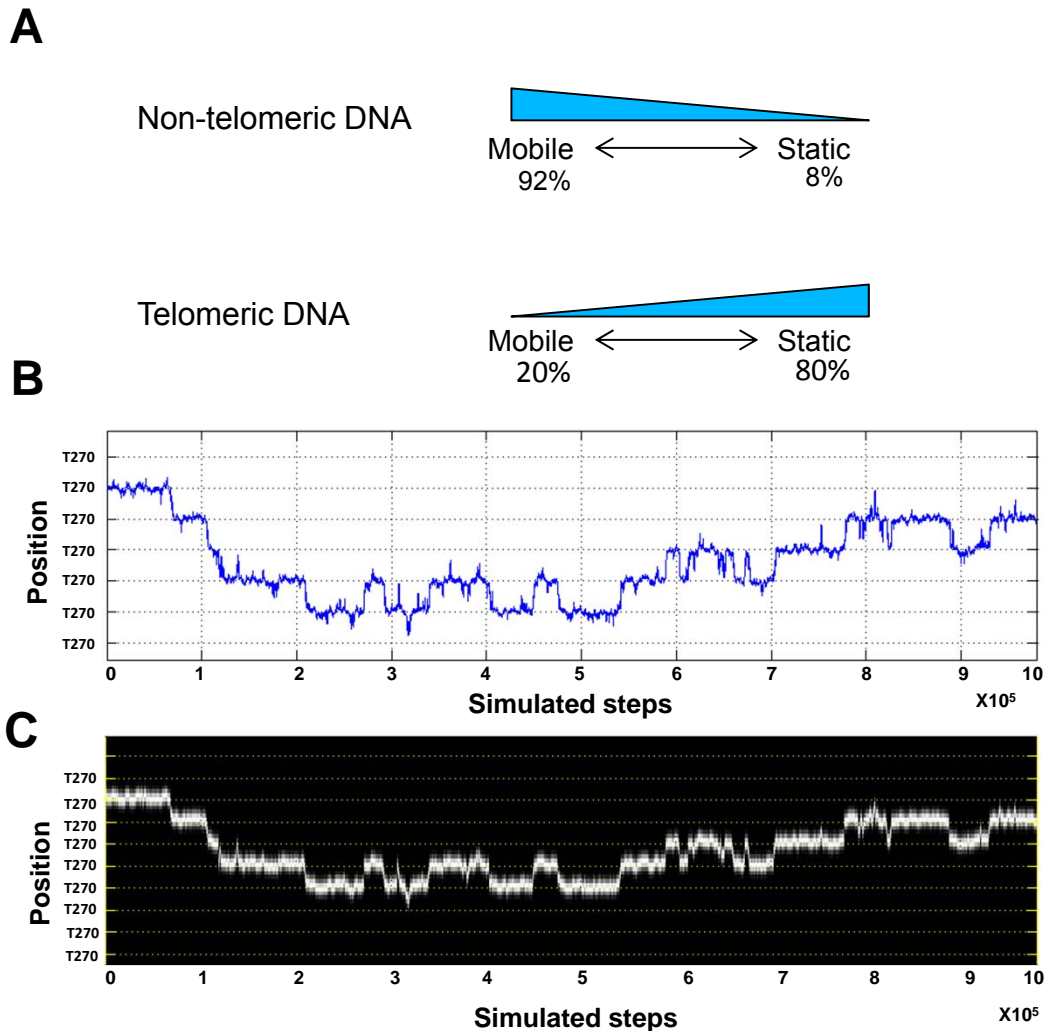
Supplementary Figure S11. Monte Carlo simulations of two-state DNA binding by SA1 on the DNA substrate with alternating telomeric and non-telomeric regions. (**A**) SA1 is hypothesized to exist in one of two DNA binding states: mobile or static. The static period is exponentially distributed with a duration of ten steps. The DNA substrate used in the simulations mimics the ligated T270 DNA (1.6 kb telomeric sequences spaced 3.8 kb apart by non-telomeric regions, Fig. 2A). (**B**) The positional trace of a simulated SA1 molecule on DNA mimicking ligated T270 DNA tightropes with alternating telomeric and non-telomeric regions. (**C**) An artificial kymograph created by converting each positional step in (B) to a Gaussian distribution. The horizontal grid lines correspond to the telomeric regions. The stepping rate is ~173000 s^{-1} for a diffusion constant of 1×10^{-3} $\mu m^2 s^{-1}$. Since the equilibrium is rapid and dynamic even on telomeric DNA, SA1 continues to diffuse over telomeric regions, however much more slowly.